Journal of Medicinal Chemistry

pubs.acs.org/jmc

Article

A Rationally Designed Novel Bifunctional Human TNF-α- and Janus Kinase-Targeted soloMER Drug Conjugate (SDC) with a Neutrophil Elastase Cleavable Linker Delivering Inflammation Site-Specific Release of Payload

Euan Murray,[‖] Stella Priyanka,[‖] Julia Martinez-Fraile,[‖] Ruslan Grygorash, Mohannad Idress, Luke C. Brownbridge, Stella Glavina, Nicolas Camper, Robert Boyd, Andrew J. Porter, Caroline J. Barelle, and Obinna C. Ubah*

Cite This: J. Med. Chem. 2026, 69, 9664−9679

Read Online

ACCESS | Metrics & More | Article Recommendations | Supporting Information

ABSTRACT: Antibody−drug conjugates have been used predominantly in oncology, but their potential in inflammatory disease remains largely unexplored. Here, we describe ELN28-135-01, a soluble TNF-α-targeted soloMER drug conjugate that extends this concept to immune-mediated inflammatory disease. ELN28-135-01 binds soluble TNF-α enriched at inflamed sites and delivers the Janus kinase inhibitor tofacitinib through a neutrophil elastase-cleavable linker, thereby coupling cytokine targeting with inflammation-triggered payload release. We report its rational design and synthesis, demonstrate selective linker cleavage in vitro and in vivo, and show that the conjugate retains potent TNF-α neutralization while enabling protease-dependent JAK inhibition. In human PBMC assays and preclinical models of acute and chronic inflammation, ELN28-135-01 achieved superior pharmacodynamic control compared with nonconjugated anti-TNF-α comparators while minimizing exposure to free tofacitinib. These findings support soluble cytokine-directed soloMER® drug conjugates as a strategy for site-restricted dual-node inflammatory pathway modulation with the potential to improve efficacy and reduce JAK inhibitor toxicities.

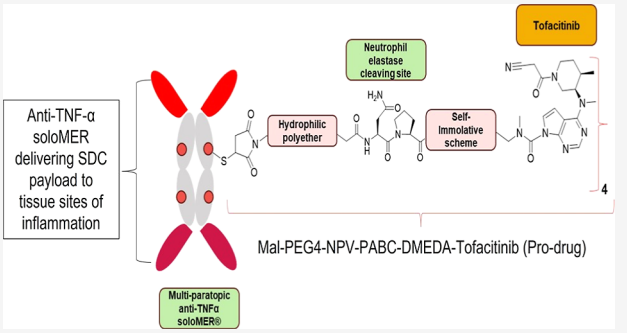

INTRODUCTION

Immune-mediated inflammatory diseases (IMIDs), including rheumatoid arthritis (RA), psoriasis (PsO), psoriatic arthritis (PsA), hidradenitis suppurativa (HS), and inflammatory bowel disease (IBD), comprise a heterogeneous group of chronic disorders whose incidence and prevalence continue to rise globally.[1] IMIDs are associated with profound impairment of health-related quality of life, increased risk of premature mortality, and escalating direct and indirect healthcare costs. Dysregulated signaling by the pro-inflammatory cytokine tumor necrosis factor (TNF-α) is a central and validated driver of pathology in IMID.[2] The advent of monoclonal antibody therapy specific for TNF-α has proven to be a successful therapeutic strategy.[3] Agents such as adalimumab (Humira), infliximab (Remicade), and golimumab (Simponi) bind TNF-α and neutralize its cell signaling function dampening its pro-inflammatory response. However, despite their success, current anti-TNF-α therapies are limited by primary nonresponse, secondary loss of response, immunogenicity, and serious adverse events, and a significant proportion of patients either do not achieve or do not sustain adequate disease control. These observations, together with evidence of pathway redundancy and compensatory signaling within the inflammatory network, highlight the intrinsic constraints of monospecific cytokine inhibition and support the rationale for multinode pathway modulation strategies to achieve more effective and durable disease remission.[4−7]

The Janus kinase-signal transducer and activator of transcription (JAK-STAT) pathway integrates signals from multiple cytokine receptors and thereby represents a complementary leverage point to TNF-α neutralization for broad immunomodulation of disease.[8] Ligand engagement activates receptor-associated JAKs, which phosphorylate receptor cytoplasmic tails and recruit STATs. Phosphorylated STATs then dimerize and translocate to the nucleus to drive transcription of key pro-inflammatory cytokines, such as IL-12 and IL-23. Small-

Received: February 16, 2026
Revised: March 24, 2026
Accepted: March 27, 2026
Published: April 7, 2026

https://doi.org/10.1021/acs.jmedchem.6c00532
J. Med. Chem. 2026, 69, 9664−9679

molecule JAK inhibitors (JAKi), including tofacitinib, filgotinib, and upadacitinib, have demonstrated clinical benefit across several IMIDs.[9−12] However, as with anti-TNF-α biologics, the utility of JAKi is constrained by efficacy plateaus and off-target safety liabilities. Regulatory concerns about dose-dependent serious adverse events, including major adverse cardiovascular events, malignancy, venous thromboembolism, and mortality, led to the addition of boxed warnings for tofacitinib, baricitinib, and upadacitinib.[13] Thus, although pharmacological JAK inhibition remains an attractive strategy for modulating disease-relevant immune circuits, its therapeutic index is limited by systemic exposure at doses required for robust target engagement. Rational, site-restricted delivery of therapeutically relevant concentrations of JAKi, specifically within inflamed tissues, while minimizing off-target systemic exposure, offers a compelling opportunity to retain efficacy while mitigating these serious adverse events.

Recent progress in immunology ADC strategies provides clinical and preclinical precedent for antibody-guided delivery of potent immunomodulators to reduce systemic liabilities. Notably, ABBV-3373 couples the anti-TNF antibody adalimumab to a glucocorticoid receptor modulator (GRM) and demonstrated clinical activity in RA consistent with targeted glucocorticoid delivery.[14] More recently, Lifordi's LF-200 is a VISTA-targeted ADC that delivers a glucocorticoid payload to immune cells using a protease-cleavable linker and has entered first-in-human evaluation (NCT07207954). Together, these programs support the feasibility of targeted small-molecule delivery in IMIDs while motivating extension to alternative payload classes (e.g., JAK inhibitors) and to inflammation-gated extracellular activation mechanisms.

Neutrophil infiltration is a common histopathological feature across IMID and is accompanied by high local activity of serine proteases such as neutrophil elastase (NE).[15−17] This inflammatory protease milieu can be harnessed for site-specific payload release, utilizing appropriately engineered drug conjugates.[18,19]

SoloMER® molecules are robust, easy-to-engineer and developable single-domain biologics with differentiated structure, evolution, and antigen-binding sites, when compared to classical antibodies and VHHs.[20−25] We previously described ELN22-108, an anti-TNF-α Quad-X soloMER that demonstrated superiority to adalimumab in multiple gold-standard efficacy studies.[26,27] ELN22-108 comprises two distinct anti-TNF-α binding domains fused to the N- and C-termini of a human Fc, yielding a superpotent and high affinity quadravalent anti-TNF-α biologic. X-ray cocrystallization studies showed that the D1 and C4 domains engage novel epitopes relative to the current anti-TNF-α landscape, and that these epitopes are selectively presented on soluble TNF-α (sTNF-α). Consequently, ELN22-108 does not bind transmembrane TNF-α (tmTNF-α); therefore, it presents a safer anti-TNF-α-targeted approach, that is also likely to elicit less anti-drug antibody (ADA)-mediated loss of response by evading tmTNF-α-mediated internalization of bound drug.[20,28]

These considerations led us to the hypothesis that coupling and delivering both high-avidity sTNF-α neutralization and spatially restricted JAKi within inflamed, neutrophil-rich tissues could deliver dual-node pathway modulation, while widening the therapeutic window of JAK inhibition. By using a TNF-α-targeted soloMER-Fc scaffold and an NE-cleavable linker conjugated to a JAKi, we hypothesized that therapeutically meaningful local concentrations of JAKi could be generated specifically at disease sites, while systemic levels would remain below thresholds associated with serious adverse events. This soloMER drug conjugate (SDC) concept is designed to exploit both the molecular specificity of sTNF-α targeting and the enzymatic microenvironment of inflamed tissues to achieve precise, potent, on-site pharmacological activation.

Here, we report the rational design of ELN28-135-01, an anti-TNF-α SDC in which the JAKi tofacitinib is conjugated via a human NE-cleavable linker, thereby coupling cytokine neutralization with locally activated JAK inhibition. Site-specific cysteine engineering at positions S239 and S442 (EU numbering) of human IgG1 Fc enables controlled linker-payload conjugation without perturbing antigen recognition or FcRn binding.[29−31] This strategy yields a homogeneous conjugate with a defined drug-to-antibody ratio (DAR) and consistent biophysical attributes, protease-triggered activation, and superior in vivo efficacy relative to appropriate controls. We further examined species differences in linker cleavage to guide translational model selection and inform future pharmacokinetic and pharmacodynamic (PK/PD) evaluations. Collectively, these data establish ELN28-135-01 as a first-in-class, multimechanism soluble TNF-α-targeted SDC and provide a delivery platform for exploiting neutrophil-mediated proteolysis to safely deploy JAK inhibition into immune-mediated inflammatory disease areas in the body.

RESULTS

Quad-X soloMER Design, Expression, and Purification

ELN22-108, described previously, was used as the parental scaffold for ELN22-135, the biologic component of the SDC evaluated here.[26,27] ELN22-135 incorporates engineered cysteines S239C and S442C (EU numbering) within the human IgG1-Fc CH2 and CH3 domains to enable site-specific conjugation; these positions support linker-payload attachment without interfering with antigen and Fc interactions.[29−31] Relative to ELN22-108, ELN22-135 is length-minimized by removing the IgG1-Fc N-terminal $(Gly_4Ser)_3$ linker and reducing the IgG1 Fc C-terminal linker from five repeats to one Gly_4Ser. An isotype control, ELN0-2V-135, was generated by replacing the D1 and C4 anti-TNF-α soloMERs with the nonbinding 2V soloMER,[32,33] at both the N- and C-termini of the Quad-X backbone, while retaining the identical Fc engineering (S239C, S442C). Codon-optimized gene constructs were transiently transfected into CHO cells for expression. Following a single purification step, both ELN22-135 and ELN0-2V-135 were obtained as predominantly monomeric species with 92−96% purity by SEC-HPLC (Figures S1 and S2).

Linker-Payload Design

For simplicity, we have used the terminology drug-to-antibody ratio (DAR) although the soloMERs are strictly antibody-like binding domains. The site-specific conjugation approach results in the formation of conjugates with a well-defined DAR, leading to homogeneous biophysical and biological properties. In this study, the two cysteines engineered in the Quad-X soloMER allowed the formation of DAR 4.0 conjugates. To generate conjugates with high stability in systemic circulation, a maleimide group coupled through its nitrogen to a PEG4 chain was used for conjugation of the linker payload to the Quad-X. To enable efficient payload release at the site of inflammation, a Asn-Pro-Val (NPV) tripeptide motif cleavable at its C-terminus by neutrophil

https://doi.org/10.1021/acs.jmedchem.6c00532
J. Med. Chem. 2026, 69, 9664−9679

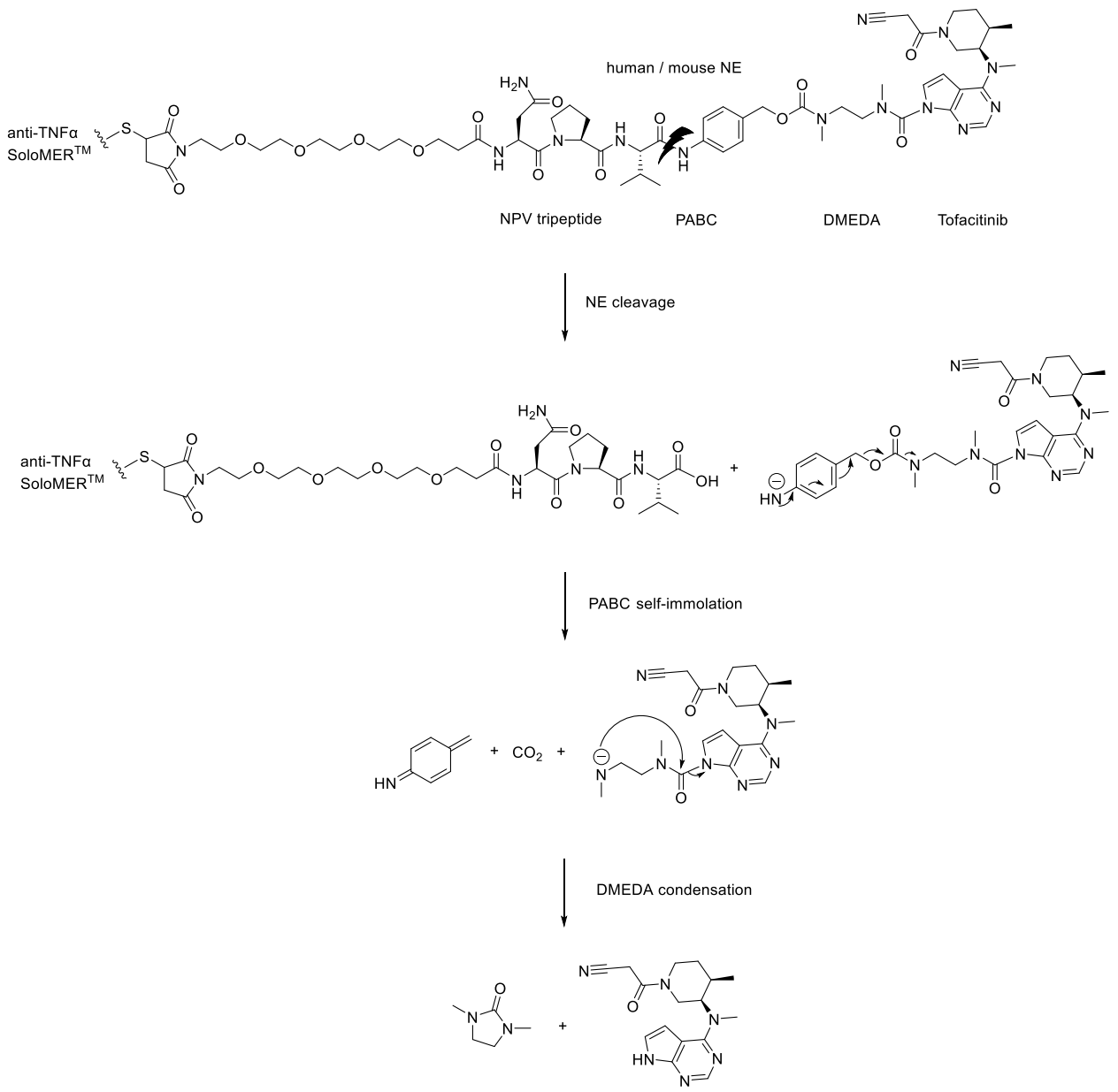

Figure 1. Predicted tofacitinib payload release mechanism following linker cleavage by neutrophil elastase.

elastase (NE), an enzyme found at high concentrations at inflammation sites,[17] was engineered into the conjugation linker. NPV tripeptide was selected as a compact, well-characterized neutrophil elastase substrate (cleaved C-terminal to Val) to provide an inflammation-associated enzymatic trigger for extracellular payload release and subsequent payload activation, as first demonstrated in an oncology ADC linker design.[19] Consistent with this rationale, elevated NE-positive infiltrates/activities have been reported in neutrophil-rich IMIDs.[34−36] The NPV tripeptide was coupled to the indole nitrogen of the JAK inhibitor tofacitinib by a tandem of self-immolative moieties, comprising a *p*-aminobenzyl alcohol (PAB) group and a *N*,*N*′-Dimethylethylenediamine (DMEDA) group, connected via a carbamate bond. The self-immolative PABC-DMEDA moiety was used to promote rapid regeneration of the native payload from an *N*-linked handle.[37] The resulting cascade leading to tofacitinib release as a free payload following linker cleavage by NE is described in Figure 1.

Synthesis of Mal-PEG4-NPV-PABC-DMEDA-Tofacitinib Linker Payload

The strategy for linker-payload synthesis is described in Figure 2. First, the Fmoc-NPV-PAB−OH intermediate 3 was assembled through a series of amide coupling reactions adapted from published procedures to avoid racemization of amino acids.[17] The Mal-PEG4-NPV-PAB-OH intermediate 4 was prepared in two steps, removing first the Fmoc protecting group from intermediate 3 with 10% piperidine in DMF and then coupling with commercially available Mal-PEG4-COOH. The DMEDA spacer was attached to the PAB moiety after activation as a PNP carbonate to give intermediate 6. Boc and trityl protective groups were removed simultaneously using trifluoroacetic acid (TFA) with TIPS/H_2O as a scavenger. Intermediate 7 was reacted with tofacitinib activated as a PNP carbamate derivative prepared according to other published

https://doi.org/10.1021/acs.jmedchem.6c00532
J. Med. Chem. 2026, 69, 9664−9679

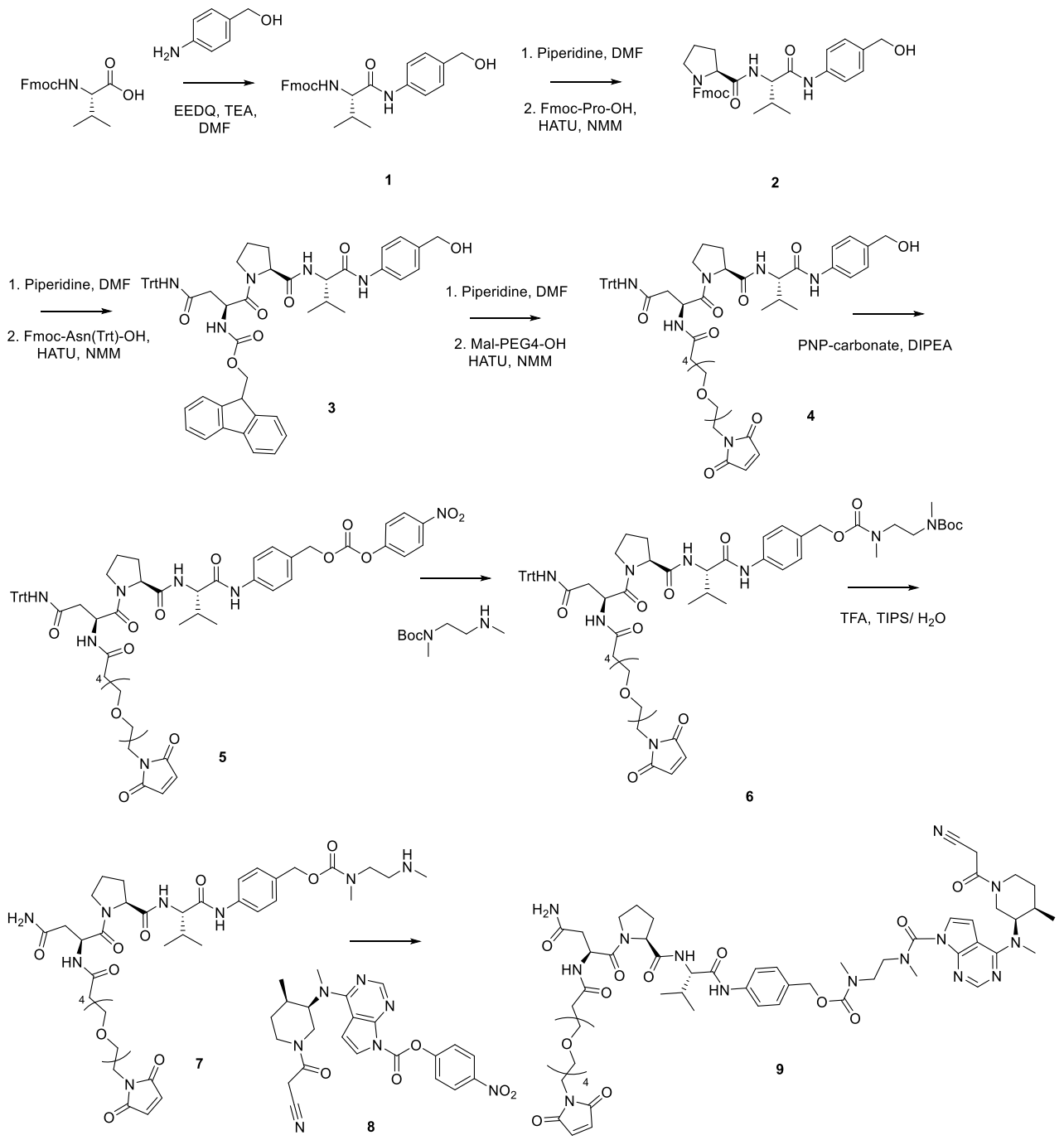

Figure 2. Mal-PEG4-NPV-PABC-DMEDA-tofacitinib linker-payload synthetic scheme.

procedures[19] to give the desired Mal-PEG4-NPV-PABC-DMEDA-Tofacitinib linker payload in high yield and excellent purity (Figures S3 and S4).

Conjugation to ELN22-135 and ELN0-2 V-135 Quad-X soloMERs

Two SDCs were generated by conjugating a maleimide linker payload to a matched pair of Quad-X soloMERs: ELN22-135 (anti-human TNF-α) and its isotype control ELN0-2V-135. Both constructs shared the same molecular design and cysteine engineering pattern (S239C, S442C) to enable site-specific conjugation. For conjugation of the linker payload, the engineered cysteines of the soloMERs were first uncapped by reduction with DTT. Reoxidation with DHAA then allowed disulfides to reform in the hinge region while leaving engineered cysteines available for conjugation. Complete conversion to DAR 4.0 conjugates was achieved with 10 to 12 eq of the maleimide linker payload per antibody after 1 h incubation at 22 °C. The conjugation process was monitored by High-Resolution Mass Spectrometry (HRMS) as shown in Figures 3 and S5. No significant differences in reactivity were observed between the two Quad-X constructs.

Preparative size-exclusion chromatography (SEC) was used to purify the conjugates, removing any residual linker payload and depleting high-molecular-weight (HMW) species present in the starting material or generated during conjugation. Both conjugates were isolated as homogeneous DAR 4.0 species with very high monomeric purity (Figures S6 and S7).

https://doi.org/10.1021/acs.jmedchem.6c00532
J. Med. Chem. 2026, 69, 9664−9679

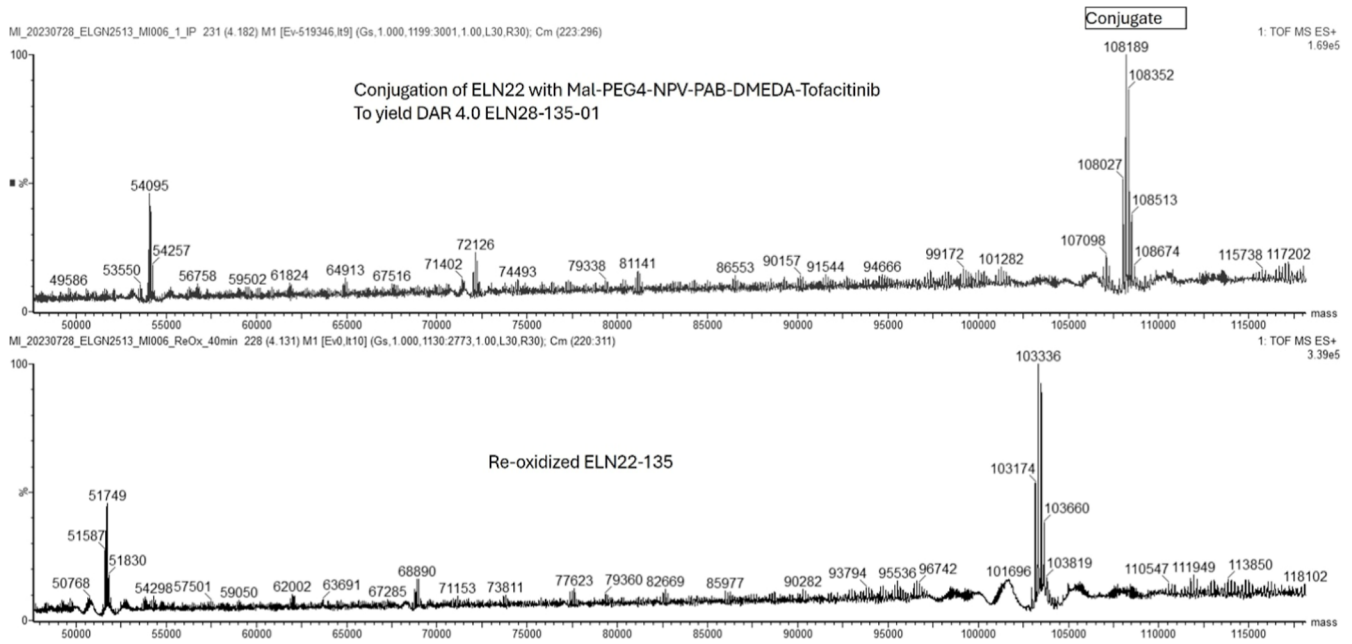

Figure 3. Mal-PEG4-NPV-PABC-DMEDA-Tofacitinib conjugation to ELN22-135 soloMER. Process monitoring by High-Resolution Mass Spectrometry. A molecular weight (MW) increase corresponding to the addition of 4 linker payloads to ELN22-135 was observed after conjugation; theoretical +1213 Da *4 = +4852 Da, measured 103,336 Da to 108,189 Da = +4853 Da.

Table 1. Neutrophil Elastase-Mediated Release of Free Tofacitinib from Mal-PEG4-NPV-PABC-DMEDA-Linker Payload, ELN28-135-01 and ELN0-2V-135-01[a]

test article	neutrophil elastase	release (%)		
		2−4 h	24 h	72 h
Mal-PEG4-NPV-PABC-DMEDA-tofacitinib	human	24*, 56#	25*, 74#	33*
	mouse	7*, 48#	15*, 51#	18*
ELN28-135-01	human	39$	47$	NA
	mouse	37$	37$	NA
ELN0-2V-135-01	human	47$	56$	NA
	mouse	33$	38$	NA

[a]Free tofacitinib was quantified by Tandem Mass Spectrometry (LC-MS/MS). For linker payload, free payload release was measured after incubating with NE for 2−4, 24, and 72 h. ELN28-135-01- and ELN0-2V-135-01 NE-mediated payload release was measured at 2 and 24 h, respectively. Values are means of duplicate measurements. Concentrations of HNE or MNE used were either 0.1 μg/mL (*), 1.7 μg/mL (#), or 4.425 μg/mL ($); NA, not assessed.

Following conjugation, ELN22-135 was designated ELN28-135-01, and the isotype control ELN0-2V-135 was designated ELN0-2V-135-01.

Evaluation of the Biophysical Properties and Plasma Stability of ELN28-135-01

We assessed the hydrophobicity of the anti-TNF-α-tofacitinib SDC ELN28-135-01 (and its isotype control ELN0-2 V-135-01) by analytical hydrophobic interaction chromatography (HIC). Conjugation at DAR 4.0 with the Mal-PEG4-NPV-PABC-DMEDA-tofacitinib linker payload increased hydrophobicity relative to the respective parent Quad-X soloMER. The relative retention time (SDC vs parent) was 1.62 min for ELN28-135-01 and 1.80 min for ELN0-2V-135, indicating a larger hydrophobicity shift for the isotype control (Figure S8A,B). Overall, linker-payload conjugation and variable domain composition appeared to be the main parameters driving hydrophobicity, consistent with the SDCs sharing the same conjugation sites on the Quad-X.

For the thermal stress study, SDCs were incubated at 37 °C for 7 days in PBS at pH 7.1 and analyzed by analytical SEC (monomeric purity) and HRMS (DAR/integrity). ELN28-135-01 and ELN0-2V-135-01 showed a modest increase in HMW species of ∼2.8−4.6% after incubation (Figure S8C,D). No deconjugation or backbone degradation was detected by HRMS for either conjugate. A mass increase of +43−44 Da was observed poststress, consistent with maleimide ring hydrolysis over time (Figure S8E,F). To investigate SDC stability in plasma, ELN28-135-01 was incubated in either human or mouse plasma at 37 °C for 7 days. After 7 days, only 0.8% and 3.2% of the total conjugated Tofacitinib was found to have been released in human and mouse plasma, respectively (Figure S8G).

Linker Payload and SDC Cleavage by Neutrophil Elastase

We performed an NE enzymatic cleavage assay to confirm the ability of the linker to be cleaved, and tofacitinib liberated as free payload. The Mal-PEG4-NPV-PABC-DMEDA-Tofacitinib linker payload was incubated with NE at 37 °C in Tris buffer (pH 7.5) and monitored over 24 to 72 h. Both human and murine NE (HNE and MNE) efficiently cleaved the linker, releasing free tofacitinib, as confirmed by LC-MS/MS

https://doi.org/10.1021/acs.jmedchem.6c00532
J. Med. Chem. 2026, 69, 9664−9679

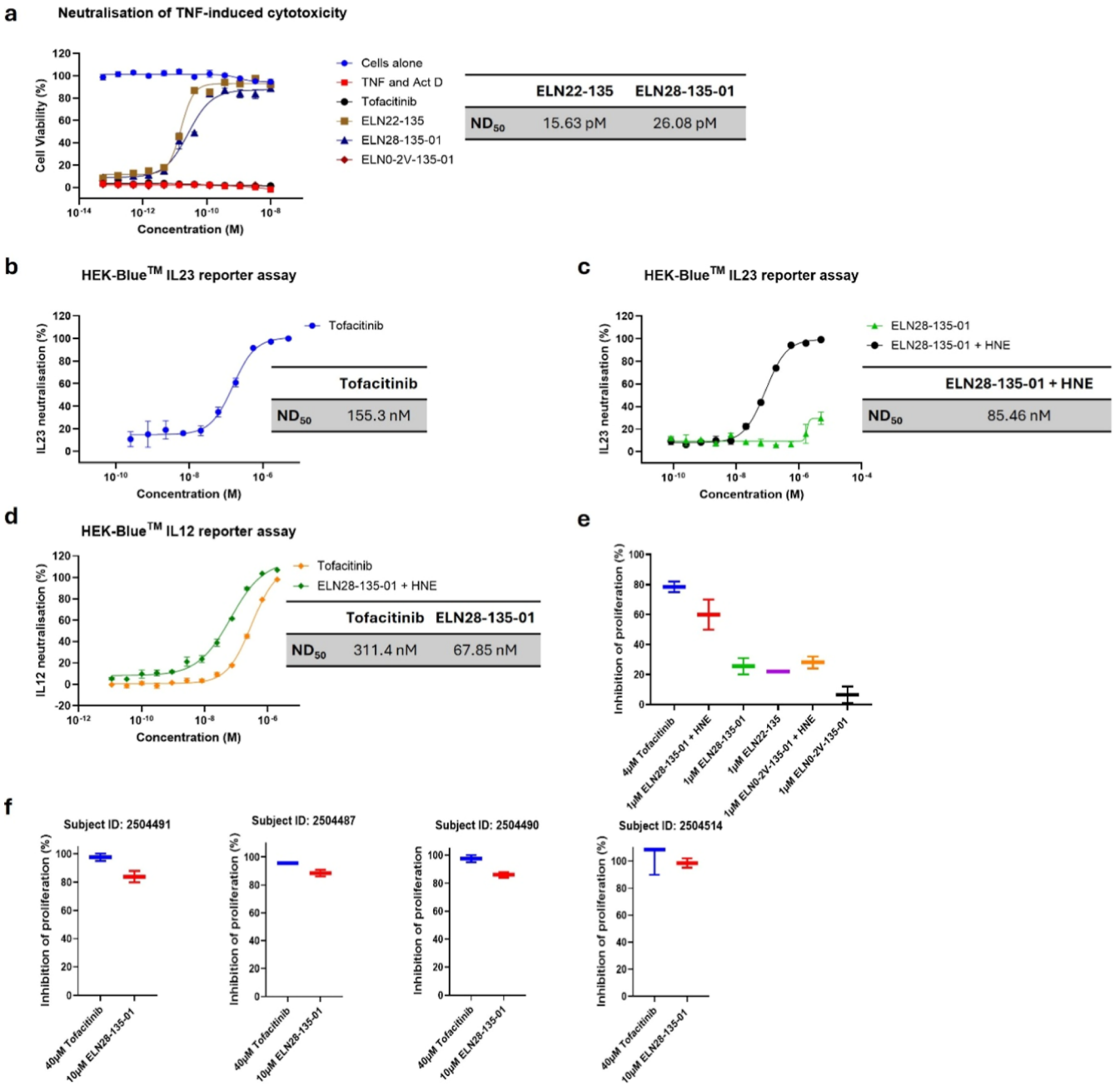

Figure 4. SDC demonstrates dual functionality. (A) Neutralization of TNF-α-mediated cytotoxicity in mouse fibrosarcoma L929 cells. (B,C) Neutralization of human IL-23-induced Tyk2-JAK2 heterodimerization and STAT3 phosphorylation in HEK-Blue IL-23 Reporter Cell. HEK-Blue IL-23 cells were treated with recombinant human IL-23 (1 ng/mL) and dilution series of (B) tofacitinib and (C) ELN28-135-01 with and without HNE (50 nM). (D) Neutralization of cynomolgus IL-12-induced Tyk2-JAK2 heterodimerization and STAT4 phosphorylation in the HEK-Blue IL-12 Reporter Cell. Data are shown as mean ± SEM (n = 2). (E) Inhibition of PHA-mediated proliferation of human PBMC samples. Human PBMCs were stimulated with PHA and treated with either tofacitinib, ELN28-135-01 in the presence or absence of HNE, ELN22-135, or ELN0-2V-135-01 in the presence or absence of HNE. (F) Inhibition of PHA-mediated proliferation of PBMCs from 4 additional donors. Human PBMCs were stimulated with PHA and treated with either tofacitinib or ELN28-135-01 in the presence of HNE. Data are shown as mean ± SEM (n = 2), ND_{50} values were calculated using four-parameter nonlinear regression.

quantification (Table 1). As expected, with high HNE concentration, a biphasic release kinetics was observed, with ∼56% of the payload liberated within the first 4 h, followed by a slower phase. After 24 h, total release reached ∼74% with HNE and ∼51% with MNE, whereas only a modest 33% of tofacitinib was released after 72 h with 0.1 μg/mL HNE. We also observed differences in the cleaving activity of HNE and MNE, which may be related to technical differences in enzyme activation and degree of activation achievable in an experimental setting; however, we demonstrated that both HNE and MNE can cleave the NPV motif to release free tofacitinib. This is relevant when selecting and translating preclinical animal models for proof-of-concept efficacy and safety studies.

Further enzymatic cleavage assays were conducted on ELN28-135-01 and ELN0-2V-135-01. As with the isolated linker payload, the assays involved incubation with NE at 37 °C in Tris buffer at pH 7.5, with samples collected over a 24 h

https://doi.org/10.1021/acs.jmedchem.6c00532
J. Med. Chem. 2026, 69, 9664−9679

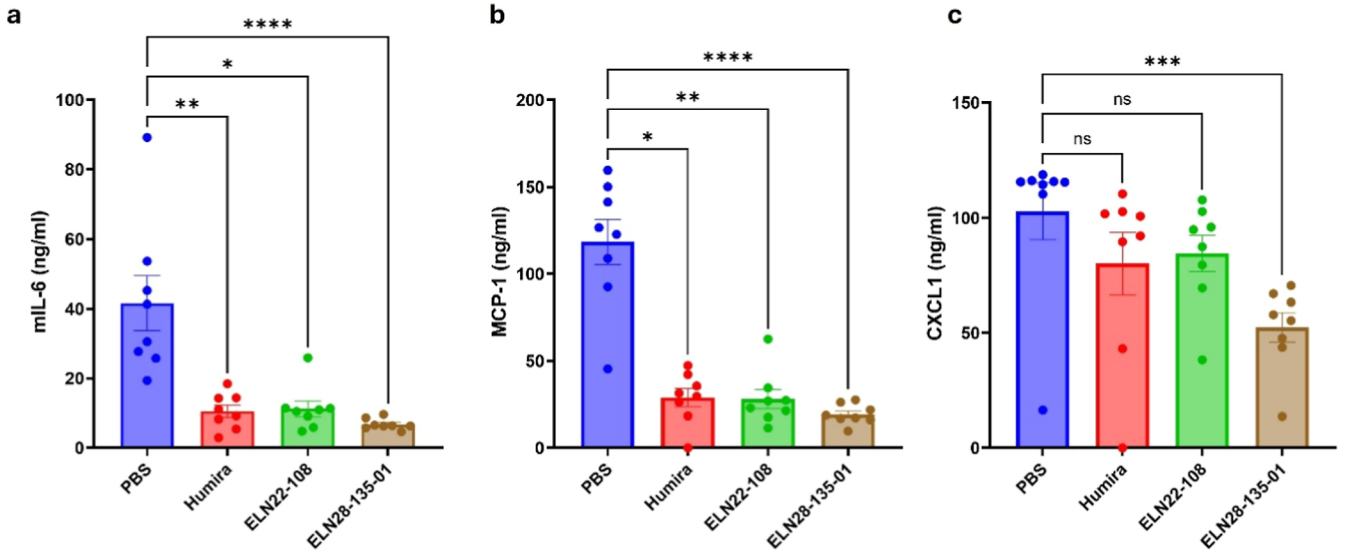

Figure 5. Attenuation of LPS-induced cytokine release in the Tg1278TNFKohTNFR1K1 mouse model. Tg1278TNFKohTNFR1K1 mice were dosed with LPS to induce an acute inflammatory response 2 h after intraperitoneal administration of anti-TNF-α biologic or SDC. Cytokine serum concentrations of (A) mIL6, (B) mMCP-1, and (C) mCXCL1 were measured by ELISA. Data are presented as mean ± SEM and statistical significance was assessed using Kruskal–Wallis test and Dunn's multiple comparison test, n = 8 mice/treatment group (*, p <0.0332; **, p <0.0021; ***, p <0.0002; ****, p <0.0001).

period and quantification of free tofacitinib payload performed via tandem mass spectrometry. All SDCs demonstrated the ability to release free payload upon incubation with NE (Table 1). Approximately 50% of the total payload initially conjugated to the Quad-X was released during the assay with HNE, with a slower release phase observed after the 2 h time point. Consistent with results from the isolated linker-payload assay, MNE yielded a lower overall payload release. No significant differences in payload release efficiency were observed between SDC constructs. Overall, these enzymatic cleavage assays validated the linker design and confirmed that the SDCs are capable of releasing tofacitinib in its active form in the presence of NE.

Functional Characterization of ELN28-135-01 and ELN0-2 V-135-01

In Vitro Functionality of SDC. Prior to conjugation, the engineered Quad-X molecules containing S239C and S442C mutations were evaluated to confirm retention of their biological activity. These modified constructs demonstrated comparable binding affinity to TNF-α relative to the parental ELN22-108 Quad-X molecule by Biolayer Interferometry (BLI) (Figure S9). Following bioconjugation with tofacitinib, the resulting SDC ELN28-135-01 maintained high-affinity binding to TNF-α in the picomolar range (Figure S9), indicating that neither the site-specific mutations nor the conjugation of Mal-PEG4-NPV-PABC-DMEDA-Tofacitinib linker payload impaired target engagement.

The L929 cytotoxicity assay, a well-established method for assessing potency of anti-TNF-α biologics,[26,27] was used to evaluate the functional integrity of the SDC. The conjugated molecules effectively neutralized TNF-α-induced cytotoxicity in L929 murine fibrosarcoma cells, with potency comparable to their unconjugated species (Figure 4A). In contrast, the isotype control SDC, ELN0-2V-135-01, and free tofacitinib were inactive in this assay. These findings, together with the BLI data, confirm that conjugation to tofacitinib did not compromise the TNF-α neutralizing activity of the biologic component.

To assess the release and functional activity of the tofacitinib payload, HEK-Blue human IL-23 reporter cells were employed. In this system, IL-23 stimulation via the IL12Rβ1:IL23R receptors results in Tyk2 and JAK2 heterodimerization and subsequent phosphorylation of STAT3. The latter then leads to the production of secreted embryonic alkaline phosphatase (SEAP), which is quantifiable by colorimetric detection. Free tofacitinib inhibited IL-23-induced STAT3 phosphorylation with an IC_{50} of 155 nM (Figure 4B). ELN28-135-01 inhibited STAT3 phosphorylation only in the presence of HNE with IC_{50} values of 75 nM (Figure 4C). As expected, in the absence of HNE, conjugated tofacitinib payload remained inactive, supporting the notion that the observed inhibitory effect of the SDCs is only attributable to JAK inhibition and not TNF-α inhibition. Furthermore, ELN28-135-01 inhibited cynomolgus IL-12-induced Tyk2-JAK2 heterodimerization and STAT4 phosphorylation in HEK-Blue human IL-12 reporter cells, again only in the presence of HNE (Figure 4D). These results support the hypothesis that active tofacitinib will be selectively released at sites of inflammation where NE is present, thereby limiting systemic exposure and reducing off-target effects.

To investigate the dual functionality of ELN28-135-01, we analyzed its ability to inhibit phytohemagglutinin-L (PHA)-induced proliferation of healthy human PBMCs. PHA is a mitogen that stimulates immune cell proliferation and cytokine release via several mechanisms, including the TNF-α and JAK/STAT signaling pathways. The isotype control SDC, ELN0-2 V-135-01, demonstrated ~30% inhibition only in the presence of HNE, indicating successful release of active tofacitinib. In the absence of HNE, both the unconjugated anti-TNF-α Quad-X ELN22-135 and SDC ELN28-135-01 showed comparable inhibition of PHA-induced proliferation, confirming preserved anti-TNF-α activity. However, in the presence of HNE, ELN28-135-01 exhibited enhanced inhibition (~60%), consistent with dual target engagement (Figure 4E). The efficacy of ELN28-135-01 was further investigated in PBMCs

https://doi.org/10.1021/acs.jmedchem.6c00532
J. Med. Chem. 2026, 69, 9664−9679

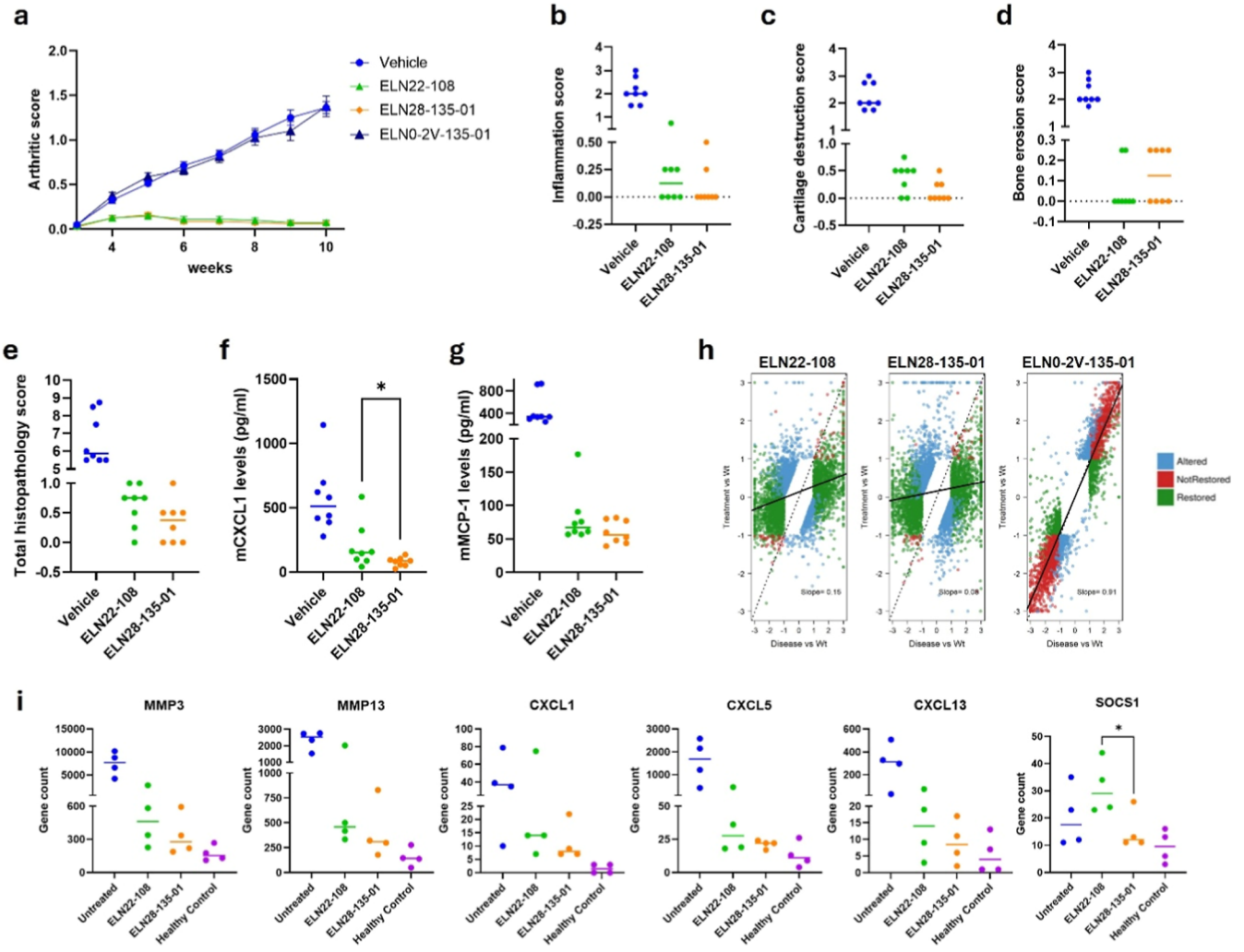

Figure 6. Efficacy of ELN28-135-01 in a Tg197 transgenic mouse model of arthritis. Tg197 mice were treated with ELN22-108, ELN28-135-01, and ELN0-2V-135-01 for 7 weeks starting at week 3. Effect of test articles on (A) in vivo arthritic score, (B) inflammation score, (C) cartilage destruction score, (D) bone erosion score, and (E) total histopathology score. (F) Mouse CXCL1 and (G) MCP-1 protein levels in serum. (H) 2D scatterplots comparing gene expression modulation. (I) Restoration of expression levels (gene counts) for genes involved in the JAK/STAT signaling pathway. Data for the arthritic score are presented as mean ± SEM (n = 10). For the rest of panels, data are presented as a scatter plot, with the median indicated by a line (n = 8). Statistical significance was assessed using an unpaired t-test with Welch's correction (*, p <0.05).

derived from four additional healthy donors. Cells were stimulated with PHA and treated with either 40 μM tofacitinib or 10 μM ELN28-135-01 in the presence of 50 nM HNE for 72 h. All donor samples responded to SDC treatment, showing inhibition of proliferation higher than 80% (Figure 4F). Although equimolar concentrations of free tofacitinib and conjugated SDC were used in the PHA-PBMC proliferation assay, we do not anticipate payload release exceeding 50% within the 72 h time frame. This is primarily due to the significantly lower concentration of HNE employed in the cell-based assay compared to that used in the in vitro enzymatic cleavage experiments (Table 1).

In Vivo Functionality of SDC. In a human TNF-α transgenic LPS-induced acute inflammation mouse model (Tg1278TNFKohTNFR1K1), ELN28-135-01 was compared with monospecific anti-TNF-α controls adalimumab/Humira (Batch 1163571, purchased from Evidentic GmbH, Germany) and the parental ELN22-108. Following dosing and LPS challenge, plasma mIL-6, mMCP-1, and mCXCL1 were quantified by ELISA (Figure 5). Across mIL-6 and mMCP-1, ELN28-135-01 produced the greatest reduction in mIL-6 and mMCP-1 (lowest p-values) and showed tighter cytokine control across animals than comparators (Figure 5A and B). In addition, mCXCL1 suppression by ELN28-135-01 was significantly greater than adalimumab or ELN22-108 (Figure 5C). Collectively, these data from an acute inflammation model indicate rapid in situ release of free tofacitinib and demonstrate the superior efficacy of ELN28-135-01.

In addition, the efficacy of ELN28-135-01 and ELN22-108 was compared in a TNF-α transgenic Tg197 mouse model of polyarthritis, where the inflammation was primarily localized in the ankle joint. Treatment with both ELN22-108 and ELN28-135-01 at 3 mg/kg completely resolved the clinical arthritic score (Figure 6A), consistent with previously published data demonstrating the efficacy of ELN22-108.[27] In this model, the disease is mainly driven by TNF-α,[7,38] and therefore, the impact of JAK inhibition on the clinical arthritic score is expected to be minimal but should be detectable by histopathological examination and multiomics analysis of the ankle joint tissue. Using these metrics, ELN28-135-01 was shown to be superior to ELN22-108. The inflammation score in the ankle joints (Figure 6B) showed complete inflammation

https://doi.org/10.1021/acs.jmedchem.6c00532
J. Med. Chem. 2026, 69, 9664−9679

resolution in 75% of the ELN28-135-01-treated mice, compared to 50% for ELN22-108 (Δ25%). In addition, treatment with ELN28-135-01 significantly reduced the cartilage destruction score compared to ELN22-108 (Figure 6C). No differences between ELN22-108 and ELN28-135-01 were observed in bone erosion (Figure 6D). Taking the three individual scores together, treatment with ELN28-135-01 demonstrated a greater reduction in the total histopathology score in the ankle joints of these mice when compared to ELN22-108 (Figure 6E), supporting its dual mechanism of activity, enhancing potency, and delivering greater therapeutic effect.

Next, we investigated the concentration of two disease-associated cytokines, CXCL1 and CCL2 (MCP-1), in the serum of these mice. While both ELN22-108 and ELN28-135-01 reduced CXCL1 protein levels, ELN28-135-01 showed a significantly superior effect (Figure 6F). Similarly, ELN28-135-01 showed a greater reduction than ELN22-108 in the expression levels of MCP-1, achieving in 100% of the ELN28-135-01-treated mice, serum levels lower than 80 pg/mL, compared to 75% of ELN22-108-treated animals (Δ25%) (Figure 6G).

Finally, the efficacy of both ELN22-108 and ELN28-135-01 was compared at the molecular level by performing RNA-Seq analysis on the ankle joints. A total of 2736 genes were identified as differentially expressed genes (DEGs) in the disease by comparing the expression levels of 10 week PBS-treated mice to 10 week wild-type mice. Differences in the expression levels of these genes were compared for ELN22−108-, ELN28-135-01-, and ELN0-2V-135-01-treated mice and results were represented in two-dimensional scatterplots (Figure 6H). In these graphs, regression lines showed the deviation of the treatment profile from the untreated or vehicle-treated group. A high positive slope demonstrated correlation with the disease and a lack of response to treatment, whereas a small slope with a near horizontal regression indicated effective treatment with a restoration of the wild-type profile. ELN28-135-01 demonstrated a 2-fold superiority over ELN22-108 in restoring the ankle joints of treated mice to a healthy, nondiseased state. In contrast, mice treated with ELN0-2V-135-01 showed no signs of tofacitinib activity, supporting a TNF-targeted mechanism of action for ELN28-135-01. As a next logical step, the capability of both ELN22-108 and ELN28-135-01 to modulate the expression levels of genes implicated in the JAK/STAT signaling pathway was determined. ELN28-135-01 outperformed ELN22-108 in restoring the expression levels of MMP3, MMP13, CXCL1, CXCL5, CXCL13, and SOCS1 to near-normal levels (Figure 6I). While providing indirect evidence, these results strongly suggest that ELN28-135-01 arrived as an intact molecule in the ankle joint and that tofacitinib was then released into the inflamed tissue. Overall, treatment with ELN28-135-01 in this chronic (predominantly sTNF-α driven) polyarthritis model resulted in more consistent disease control across all mice, demonstrating enhanced therapeutic efficacy at both the tissue and molecular levels.

Altogether, these results demonstrated a dual mechanism of activity for ELN28-135-01 in vivo in both LPS-induced acute and chronic inflammation mouse models, showing its superior therapeutic benefit and strongly supporting its further clinical development.

DISCUSSION AND CONCLUSIONS

Here, we describe the development and characterization of ELN28-135-01, a multifunctional soloMER drug conjugate (SDC) that, to our knowledge, represents a first-in-class approach integrating two clinically validated but individually imperfect therapeutic strategies, namely: TNF-α neutralization and JAK-STAT pathway inhibition. While both anti-TNF-α biologics and JAK inhibitors are well established in the management of IMIDs, their broader utility is constrained by incomplete response rates, secondary loss of efficacy, and dose-limiting safety concerns. ELN28-135-01 was conceived to address these constraints by safely targeting and inhibiting multiple complementary nodes within the inflammatory network and relying on a site-of-inflammation restricted cleavage and release of JAK inhibitor payload, tofacitinib. In this modality, tofacitinib is first carried inertly (pro-drug) on an anti-TNF-α Quad-X-Fc scaffold and is released only following NE-mediated linker cleavage in inflamed, neutrophil-rich tissues. Release is then followed by a chemically rapid but self-limiting immolative step to convert the pro-drug to an active form. This design aims to generate therapeutically meaningful JAK inhibition at the disease site while maintaining very low levels of free drug in the systemic circulation, widening the therapeutic index relative to current, orally dosed JAK inhibitors.

From a developability perspective, ELN28-135-01 exemplifies how precise conjugation chemistry can be used to build multi-functional biologics with predictable pharmacology. Site-specific cysteine engineering at positions S239 and S442 of the human IgG1 Fc enabled controlled conjugation of four linker-payload moieties, yielding a homogeneous SDC with a defined DAR of 4.0. As expected, conjugation of four hydrophobic linker-payload units increased the overall hydrophobicity, but the conjugate retained high monomeric purity and showed no evidence of aggregation under thermal stress for at least 7 days. This combination of site-specific conjugation, controlled DAR, and preserved biophysical integrity supports both robust manufacturing and predictable consistent in vivo behavior. These developability attributes align with the emerging class of immunology-focused ADCs designed to concentrate potent immunomodulators in immune/inflamed tissues, exemplified by AbbVie's ABBV-3373 and Lifordi's LFD-200.[39,40]

Compared with ABBV-3373 and LFD-200, which primarily aim to deliver glucocorticoid activity to immune/inflamed compartments, ELN28-135-01 is differentiated by its payload class and activation gate. First, ELN28-135-01 delivers a JAK inhibitor (tofacitinib) to modulate the JAK-STAT signaling (and thus multiple cytokine circuits) in a manner complementary to TNF-α neutralization, rather than recapitulating glucocorticoid pharmacology. Second, payload liberation is gated by extracellular NE activity enriched in neutrophil-rich inflammatory loci, reducing reliance on target-mediated internalization as the sole route to payload activation. Collectively, these features suggest that ELN28-135-01 may offer a distinct route to local multinode pathway modulation with minimized systemic free-drug exposure, complementing the glucocorticoid-ADC concept represented by ABBV-3373 and LFD-200.[39,40].

The linker-payload design incorporates a dual self-immolative cascade to couple enzymatic specificity with efficient payload unmasking. Cleavage assays with human NE (HNE) and mouse NE (MNE) confirmed that ELN28-135-01

https://doi.org/10.1021/acs.jmedchem.6c00532
J. Med. Chem. 2026, 69, 9664−9679

undergoes efficient proteolysis, with subsequent self-immolation of PABC and DMEDA motifs leading to release of free, pharmacologically active tofacitinib. Quantitatively, HNE generated ∼74% of the expected tofacitinib after 24 h compared with 51% for MNE under identical conditions, indicating successful activation in both systems. While this pattern is consistent with a species difference that should be considered when selecting and interpreting preclinical models, it may also in part reflect the more involved procedure required for MNE activation in plasma. At the experimental HNE and MNE concentrations of 4.4 μg/mL, which falls within the range reported for certain inflammatory conditions,[17,41−44] payload release proceeded in a time-dependent manner over 24−72 h without reaching complete payload release. These data support a sustained-release paradigm in which the conjugate delivers a controlled release of tofacitinib over time, aligning with the goal of maintaining local pharmacological pressure at inflamed sites while avoiding a rapid, systemic "high-concentration dump" of free (potentially toxic) drug.

This controlled release is further supported by the physiological and pathological contexts of NE activity. NE activity is tightly controlled by a high systemic level of endogenous antiproteases, primarily alpha-1-antitrypsin (α_1-AT), which is abundant in the serum at ∼1.5−3.5 g/L. This regulated balance between NE and α_1-AT confines NE's activity to the immediate vicinity of the inflammatory foci.[17,45−47] In this setting, ELN28−135−01 is expected to encounter functionally relevant NE activity predominantly in diseased tissues, and with reduced antiprotease shielding, it delivers local release of payload and potentially prolonged inflamed tissue residence time. Thus, both the biochemical properties of the linker and the spatially confined nature of NE activity work together to support the conceptual objective of site-restricted JAK inhibition with minimal systemic exposure.

We also considered the inherent liabilities of maleimide-based conjugation, particularly the balance between stabilizing succinimide ring hydrolysis and destabilizing retro-Michael deconjugation. Thiol-conjugated maleimide linkers can undergo hydrolysis to ring-opened derivatives resistant to linker-payload deconjugation, but they may also undergo retro-Michael reactions, releasing the linker payload from the antibody in circulation and potentially compromising both efficacy and safety.[48] The electronic environment of the succinimide thioether groups formed by maleimide−thiol conjugation influences their susceptibility to retro-Michael reaction relative to hydrolysis. Succinimide thioethers with electron-withdrawing N-substituents such as PEG preferentially undergo hydrolysis over retro-Michael reaction and provide stable attachment of the linker payload to the antibody.[49,50] In parallel, the local environment at the conjugation site on the antibody modulates maleimide stability and deconjugation propensity. In ELN28-135-01, the combination of PEG-substituted maleimide and carefully selected Fc conjugation sites yielded a stable conjugate as shown in the plasma and thermostability assay (7 days at 37 °C), supporting linker stability over time scales relevant for acute and subacute pharmacology. Nonetheless, potential reverse-Michael reactions will need to be fully characterized in extended stability and in vivo PK studies to confirm that systemic off-target release remains minimal under chronic dosing conditions.

In vitro analysis confirmed the functionality of both arms of the bifunctional molecule. ELN28-135-01 was comparable to the nonconjugated starting material ELN22-135, demonstrating that linker-payload conjugation had no detrimental effect on the TNF-α neutralization ability of the biologic component of the SDC. In addition, ELN28-135-01 inhibited both human IL-12- and IL-23-induced JAK2 activation but only in the presence of HNE, confirming successful release of active tofacitinib. Ex vivo studies involving human PBMC from healthy donors demonstrated the dual functionality and additive effect of the ELN28-135-01 in inhibiting PHA-induced proliferation when compared to ELN22-108 and the isotype control conjugated to tofacitinib.

The in vivo data further supported the hypothetical rationale for this SDC design. In an acute LPS-induced inflammation model (Tg1278TNFKOhTNFR1KI), ELN28-135-01 outperformed adalimumab and ELN22-108 in suppressing key inflammatory mediators such as IL6, MCP-1, and CXCL1 in plasma, aligning with the known cytokine modulation signature of tofacitinib,[51] and suggesting effective on-target activation in a neutrophil-rich inflammatory environment. While such acute models are informative for proof of concept, they underrepresent chronic, tissue-specific pathology. Accordingly, we evaluated ELN28-135-01 in the Tg197 transgenic chronic polyarthritis model, where disease is predominantly driven by soluble human TNF-α and where a 3 mg/kg dose of ELN22-108 is known to induce complete clinical disease suppression.[27] In this stringent setting, both ELN22-108 and ELN28-135-01 markedly controlled disease relative to vehicle and isotype-tofacitinib SDC controls, confirming that efficacy derives from targeted mechanisms rather than nonspecific Fc or scaffold effects. Importantly, however, ELN28-135-01 conferred more consistent and comprehensive disease control at the tissue level than ELN22-108 across all animals, with lower histopathological scores for inflammation and cartilage destruction, greater suppression of CXCL1 and MCP-1 in serum, and superior restoration of the ankle joint transcriptome toward a nondiseased state (RNA-Seq analysis). By contrast, ELN0-2V-135-01, which lacks TNF targeting, showed no evidence of tofacitinib activity in the joints, reinforcing that disease-relevant JAK inhibition in situ depends on TNF-α-directed delivery and local linker cleavage. Collectively, these data demonstrate that ELN28-135-01 not only matches but surpasses a highly efficacious, sTNF-α-selective comparator at both tissue and molecular levels, providing experimental support for the hypothesized mechanistic advantage of dual-node modulation.

Despite these very encouraging findings, several questions remain. A key next step will be to directly quantify intralesional tofacitinib concentrations and JAK-STAT pathway modulation in target tissues, thereby linking NE-mediated cleavage to molecular target engagement and downstream pharmacodynamic effects. Comprehensive biodistribution and PK/PD studies will also help to define the relationship between dose, systemic exposure to conjugated and free tofacitinib, and on-target activity in relevant organs. The species differences observed in NE-mediated cleavage highlight the need to carefully select and benchmark preclinical models and ultimately to confirm the mechanism in human tissues, including those from patients with IMIDs.

Taken together, our findings position ELN28-135-01 as a compelling proof of principle for a broader SDC philosophy in inflammatory disease, using disease-defining extracellular cues (TNF-α) and tissue-restricted enzymatic activities (NE) to gate the local delivery and activation of otherwise systemically

https://doi.org/10.1021/acs.jmedchem.6c00532
J. Med. Chem. 2026, 69, 9664−9679

constrained small-molecule immunomodulators. ELN28-135-01 achieves a favorable balance between efficacy and developability and provides a blueprint for modular extension of this approach to other payloads, targets, and indications. More broadly, this work illustrates how soloMER-based SDCs can be engineered to deliver precise, context-dependent multinode pathway modulation, with the long-term goal of achieving deeper, more durable disease control while mitigating the systemic toxicities that currently limit many targeted therapies in IMIDs and leave a significant proportion of patients without a suitable therapy option.

EXPERIMENTAL SECTION

Quad-X soloMER Production

ELN22-135 and ELN0-2V-135 Quad-X soloMER intermediates were produced by Evitria AG (Zurich, Switzerland). Mammalian expression system codon-optimized Quad-X soloMER genes were synthesized, cloned into Evitria's proprietary expression vectors, and transfected into CHO K1 cells. Expressions were carried out using their proprietary media and growth conditions. Quad-X soloMER material was purified by MabSelect SuRe affinity chromatography. Purities were measured by SEC-HPLC, endotoxin levels were measured and confirmed to be ≤0.1 EU/mg, and the sample was supplied in PBS.

ELN22-108 Quad-X soloMER was produced by Aragen (Morgan Hill, CA, USA). A mammalian expression system codon-optimized gene construct was transfected by electroporation into CHO-GS cells to generate a stable transfected mini pool. ELN22-108 was purified from the supernatant using rProteinA, yielding a protein with 94.8% purity by SEC and endotoxin level <0.008 EU/mg. The protein sample was supplied in PBS.

RP-HPLC Analysis

RP-HPLC was carried out using an ACE, Excel 2 Super C18 UHPLC column (2.1 × 75 mm, 2.0 μm) connected to a Dionex Ultimate 3000 UPLC system equipped with a Variable Wavelength Detector. The mobile phase was solvent A: water, 0.05% (v/v) TFA. A linear gradient (5−100% B in 14 min) was applied using solvent B (acetonitrile, 0.05% (v/v) TFA) at a flow rate of 0.9 mL/min to elute bound species. The column was maintained at 30 °C throughout the analysis. The analysis was carried with UV detection at 214 and 254 nm.

RP-LC-MS Analysis

LC-MS analysis was carried out on a Waters Xevo TQ-S micro triple-quadrupole mass spectrometer and a Zorbax SB-C-18 Rapid Resolution HT column (1.8 μm, 3.0 × 50 mm; Agilent) connected to a Waters Acquity Premier UPLC system. The mobile phase was solvent A (0.1% formic acid in water). A gradient (5−100% B gradient in 6 min) was applied using solvent B (acetonitrile, 0.1% formic acid) at a flow rate of 1.0 mL/min. The column was maintained at 30 °C throughout the analysis. Mass spectrometric analysis was performed in positive ion mode, scanning 100−2000 *m*/*z*.

Hydrophobic Interaction Chromatography (HIC) Analysis

HIC was carried out using a TOSOH Bioscience TSKgel Butyl-NPR column (4.6 mm × 3.5 cm, 2.5 μm), connected to a Dionex Ultimate 3000 UPLC system. The mobile phase was buffer A (1.5 M ammonium sulfate, 50 mM sodium phosphate, pH 7.0). A linear gradient (0−100% B in 10.5 min) was applied using Buffer B (20% isopropanol, 50 mM sodium phosphate, pH 7.0) at a flow rate of 1.35 mL/min to elute bound species. The column was maintained at 30 °C throughout the analysis. The analysis was carried with UV detection at 280 nm. The SDC sample was diluted to 0.1 mg/mL using HIC loading buffer (PBS: 50 mM sodium phosphate, 3 M ammonium sulfate, pH 7.0 (1:1)). Ten micrograms of sample (100 μL) were injected per analysis.

Size Exclusion Chromatography (SEC) Analysis

Analytical SEC was carried out using an ACQUITY UPLC BEH SEC column (4.6 mm × 15 cm, 200 Å, 1.7 μm) and a guard column (4.6 mm × 3 cm), connected to a Dionex Ultimate 3000 UPLC system. The mobile phase was 0.2 M potassium phosphate buffer, pH 6.8, 0.2 M potassium chloride, 15% (v/v) isopropanol. The flow rate was kept constant at 0.35 mL/min. The column was maintained at 30 °C throughout the analysis. The analysis was carried out in a 10 min isocratic elution with UV detection at 280 nm. Five micrograms of SDC were injected for analysis. The percentage of HMW species was calculated by comparing the peak area corresponding to HWM species at 280 nm to total peak area corresponding to HWM and monomeric species at 280 nm.

High-Resolution Mass Spectrometry Analysis

LC-MS analysis was carried out using a Waters XEVO G2S TOF mass spectrometer and a Waters BioResolve mAb RP Polyphenyl 450 Å (2.1 × 30 mm, 2.7 μm) column connected to a Waters Acquity H Class Ultrahigh-Performance liquid chromatography (UPLC) system. The mobile phase was buffer A (0.1% formic acid in water). A gradient (2.5 min 10% B, 10−80% B gradient in 3.5 min) was applied using buffer B (acetonitrile, 0.1% formic acid) at a flow rate of 0.4 mL/min. The column was maintained at 55 °C throughout the analysis. The SDCs were diluted to 0.05 mg/mL with LC-MS-grade water, and 10 μL of sample (0.5 μg) was injected for analysis.

Endotoxins Determination

The EndoSafe-PTS platform (Charles River) was used to determine the level of endotoxin in SDC samples according to manufacturer's instructions.

Linker-Payload Synthesis

Mal-PEG4-Asn(Trt)-Pro-Val-PAB-OH (Intermediate 4). Piperidine (1.28 mL, 13 mmol) was added to a solution of Fmoc-Asn(Trt)-Pro-Val-PAB-OH (intermediate 3) (1.17 g, 1.3 mmol) in DMF (12 mL). The reaction mixture was stirred for 1 h at room temperature (RT). DMF was then concentrated in vacuo. The oil residue was extracted with hexane (3 × 30 mL) and combined hexane extracts were discarded. The solidified residue was dried in high vacuum for 16 h and taken to the next step assuming quantitative recovery. Mal-PEG4-COOH (450 mg, 1.3 mmol) was dissolved in DMF (10 mL). The flask was cooled down to 0 °C. HATU (658 mg, 1.73 mmol) and *N*-methylmorpholine (550 mL, 5.21 mmol) were added and the mixture was stirred for 30 min. The h-Asn(Trt)-Pro-Val-PAB−OH solid was dissolved in DMF (10 mL) and added to the solution. The resulting reaction mixture was stirred at RT for 3 h. The mixture was poured in water (100 mL) and extracted with ethyl acetate (3 × 50 mL). The combined organic layers were washed with 5% citric acid aqueous solution, 5% $NaHCO_3$ solution, brined, and dried over Na_2SO_4. The crude was purified by reverse-phase C-18 column chromatography using buffer A (water: 0.05% TFA (v/v)) and buffer B (acetonitrile: 0.05% TFA (v/v)) with a gradient elution from 100:0 (v/v) to 20:80 (v/v). Fractions were combined and lyophilized to give the desired product (0.95 g, 73.1%) as an off-white solid. MS (ESI+), *m*/*z*: $[M + H]^+$ (1003.59, 100%), $[M + Na]^+$ (1025.58, 50%).

Mal-PEG4-Asn(Trt)-Pro-Val−PAB-PNP (Intermediate 5). PNP carbonate (404 mg, 1.32 mmol) and *N*,*N*-diisopropylethylamine (500 μL, 2.84 mmol) were added to a solution of Mal-PEG4-Asn(Trt)-Pro-Val-PAB−OH (950 mg, 0.95 mmol) in DMF (15 mL). The reaction mixture was stirred for 5 h at RT. DMF was concentrated in vacuo to half of the initial volume and added dropwise to diethyl ether (120 mL). The solid was filtered off and washed on filter with ether and hexane. The collected material containing some para-nitrophenol and traces of the starting material was used in the next step without further purification. The yield was assumed to be close to quantitative. MS (ESI+), *m*/*z*: $[M + H]^+$ (1168.62, 100%), $[M + Na]^+$ (1190.59, 33%).

Mal-PEG4-Asn(Trt)-Pro-Val-PABC-N-(Boc)-N,*N*′-Dimethylethylenediamine (Intermediate 6). N-(Boc)-*N*,*N*′-Dimethylethylenediamine (267 mg, 1.42 mmol) was added to a solution of crude Mal-PEG4-Asn(Trt)-Pro-Val-PAB-PNP in DMF (10 mL) and the

https://doi.org/10.1021/acs.jmedchem.6c00532
J. Med. Chem. 2026, 69, 9664−9679

reaction mixture was stirred for 4 h at RT. The reaction mixture was loaded on a reverse-phase C-18 column and purified using buffer A (water: 0.05% TFA (v/v)) and buffer B (acetonitrile: 0.05% TFA (v/v)) with a gradient elution from 85:15 (v/v) to 0:100 (v/v). Combined fractions were concentrated in vacuo and then lyophilized to give the desired product (507 mg, 43.8% for two steps). MS (ESI +), m/z: $[M + Na]^{2+}$ (1239.69, 64%), $[M\text{-Boc} + H]^{+}$ (1117.65, 100%).

Mal-PEG4-Asn(NH_2)-Pro-Val-PABC-DMEDA (Intermediate 7). TIPS (250 μL) and water (250 μL) were added to a solution of Mal-PEG4-Asn(Trt)-Pro-Val-PABC-N-(Boc)-*N*,*N*′-dimethylethylene-diamine (507 mg, 0.416 mmol) in DCM (5 mL). The flask was placed in an ice bath and TFA (4.5 mL) was added slowly. The reaction mixture was stirred for 1 h at RT and then concentrated in vacuo. The residue was purified by reverse-phase C-18 column chromatography using buffer A (water: 0.05% TFA (v/v)) and buffer B (acetonitrile: 0.05% TFA (v/v)) with a gradient elution from 100:0 (v/v) to 30:70 (v/v). Combined fractions were concentrated in vacuo and then lyophilized to give the desired product (125 mg, 34.1%) as a TFA salt. MS (ESI+), m/z: $[M+2H]^{2+}$ (438.62, 100%), $[M + H]^{+}$ (875.61, 30%).

Tofacitinib PNP Carbonate (Intermediate 8). The synthesis of Tofacitinib PNP carbonate has been previously described.[52]

Mal-PEG4-Asn(NH_2)-Pro-Val-PABC-DMEDA-Tofacitinib (Intermediate 9). Tofacitinib-PNP carbonate (40 mg, 0.085 mmol) and *N*-methylmorpholine (110 μL, 0.1 mmol) were added to a solution of Mal-PEG4-Asn(NH_2)-Pro-Val-PABC-DMEDA TFA salt (51 mg, 0.051 mmol) in DMF (2 mL). The reaction mixture was stirred for 2 h at RT and then concentrated in vacuo. The residue was purified by reverse-phase C-18 column chromatography, using buffer A (water: 0.05% TFA (v/v)) and buffer B (acetonitrile: 0.05% TFA (v/v)) with a gradient elution from 95:5 (v/v) to 20:80 (v/v). Combined fractions were concentrated in vacuo and then lyophilized to give the desired product (48 mg, 77.2%) as a white solid. Material purity was determined to be >99% by HPLC at UV 214 and 254 nm. MS (ESI+), m/z: [M+2H]2+ (607.72, 100%), [M + H]+ (1213.66, 28%).

General Procedure for Linker-Payload Conjugation to the Quad-X soloMERs

Quad-X soloMER (5.0 mg/mL, in Dulbecco's PBS, pH 7.2, 2 mM EDTA) was reduced with 15 mM DTT. After 1 h incubation at 22 °C, reduced Quad-X soloMER was buffer exchanged into PBS, pH 7.2, 2 mM EDTA by ultrafiltration/diafiltration using Vivaspin 20 centrifugal concentrators (PES membrane, 30 kDa MWCO). Quad-X soloMER at 4 mg/mL was reoxidized with 30 eq DHAA per antibody for 1 h at 22 °C. Conjugation of reduced and reoxidized Quad-X soloMER with 8.0 to 12 eq of Mal-PEG4-NPV-PABC-DMEDA-Tofacitinib linker payload per antibody was then performed. Mal-PEG4-NPV-PABC-DMEDA-Tofacitinib linker payload was prepared in DMSO (10% v/v DMSO). Quad-X soloMER was diluted to 3.0 mg/mL with Dulbecco's PBS, pH 7.2, 2 mM EDTA, mixed gently with Mal-PEG4-NPV-PABC-DMEDA-Tofacitinib linker payload and incubated at 22 °C for 1 h. The reaction mixture was then purified by preparative SEC on a HiLoad 26/600 Superdex 200 pg column equilibrated with Dulbecco's PBS, pH 7.2. The flow rate was kept constant at 2.5 mL/min. Fractions were collected and analyzed by analytical SEC. Fractions containing monomeric SDC were pooled and concentrated using Vivaspin 20 centrifugal concentrators (PES membrane, 30 kDa MWCO). Concentrated SDC samples were sterile-filtered through a 0.22 μm pore size PVDF membrane filter, quantified by UV-A280, and characterized by SEC, LC-MS, HIC, and LAL endotoxin assay. All SDC test articles are >95% pure by analytical SEC.

Neutrophil Elastase Payload Release

For neutrophil elastase payload release assays, soloMER conjugates were prepared at 6 μM into reaction buffer (100 mM Tris−HCl, 500 mM NaCl, pH 7.5 or 50 mM Tris−HCl, 1 M NaCl, pH 7.5 for HNE or MNE cleavage assays, respectively) before activated HNE or MNE was spiked to a final concentration of 4.425 μg/mL. The reaction mixtures were incubated at 37 °C and time points were collected between 0 and 24 h. The reactions were terminated by adding formic acid to a final concentration of 1% (v:v) and stored at −80 °C pending analysis.

For neutrophil elastase payload release assays with isolated linker payload, the linker payload was prepared at 4 μg/mL or 50 μg/mL into reaction buffer (100 mM Tris−HCl, 500 mM NaCl, pH 7.5, or 50 mM Tris−HCl, 1 M NaCl, pH 7.5, for HNE or MNE cleavage assays, respectively) before activated HNE or MNE was added to a final concentration of 0.1 μg/mL or 1.7 μg/mL, respectively. The reaction mixtures were incubated at 37 °C and time points were collected between 0 and up to 72 h. The reactions were terminated by adding formic acid to a final concentration of 1% (v:v) and stored at −80 °C pending analysis.

A Cathepsin C control sample was also prepared due to the requirement for MNE to be activated with this enzyme prior to use. A calibration curve was prepared with tofacitinib in reaction buffer at concentrations between 15.0 ng/mL to 1500 ng/mL with independent QC samples at 45.0, 750, and 1125 ng/mL (Figure S10, Table S1 and S2). Payload release time points, calibration standards, and QC samples were extracted and analyzed by LC-MS/MS using an Acquity UPLC in line with a Xevo TQ-S Premier mass spectrometer (Waters): 50 μL of sample was spiked with 150 μL of Fluticasone Propionate (internal standard-IS) at 1000 ng/mL in water:formic acid (100:0.1 v:v). Samples were mixed for 5 min at 900 rpm before analysis. Separation was performed using an Acquity Premier C18 (1.7 μm, 1.0 × 50 mm) column. The chromatographic method consisted of a gradient starting at 95% mobile phase A (0.1% formic acid in water) to 80% mobile phase B (0.1% formic acid in acetonitrile) over 4.75 min. Mass spectrometric analysis was performed in positive ion mode, with targeted MS/MS setup as reported in Table 2.

Table 2. Transition Monitored for LC-MS/MS Analysis

	RT (mins)	parent ion (m/z)	fragment ion (m/z)
tofacitinib	1.77	313.211	107.024
fluticasone propionate	3.56	501.155	313.196

A calibration curve was generated using the known concentration of analyte and the ratio of analyte to internal standard instrument response. A linear regression with $1/X^2$ weighing was applied and used to back calculate the sample concentration.

Plasma Stability Study

The SDC was diluted into plasma at 1 mg/mL and incubated at 37 °C for up to 168 h. Samples were collected at 0, 24, 48, 96, 144, and 168 h and stored at −80 °C pending analysis. Stability time points in human and mouse plasma (LiHep) were analyzed in a single analytical run along with calibration standards and quality control (QC) samples. A calibration curve was prepared with Tofacitinib in plasma at concentrations between 15.0 ng/mL and 1500 ng/mL with independent QC samples at (45.0, 750, and 1125 ng/mL). Incubated plasma stability time points, calibration standards, and QC samples were extracted prior to LC-MS analysis: 50 μL of sample was spiked with 150 μL of Fluticasone Propionate (internal standard - IS) at 1000 ng/mL in acetonitrile:formic acid (100:0.1 v:v). Samples were mixed for 5 min at 900 rpm before centrifugation at 2250*g*, 4 °C for 10 min in a Fresco 21 refrigerated Microcentrifuge (Thermo Scientific). After centrifugation, 100 μL of the supernatant was transferred to a clean plate well and diluted with 275 μL 0.1% formic acid in water. Samples were analyzed by LC-MS/MS for free tofacitinib quantification as described in the neutrophil elastase payload release assay.

Reagents

Actinomycin D (1229, R&D Systems), Healthy human PBMCs (Precision Medicine), HEK Blue Reporter Assay IL23 (hkb-il23, InvivoGen), HEK Blue Reporter Assay IL12 (hkb-il12, InvivoGen),

https://doi.org/10.1021/acs.jmedchem.6c00532
J. Med. Chem. 2026, 69, 9664−9679

L929 (Sigma), human IL23 (1290-IL/CF, R&D Systems), cynomolgus IL12 (10215-CL, R&D systems), human neutrophil elastase (324681, Merck), human TNF-α (TNFA-HA4211, Acro Bioscience), Phytohemagglutinin-L (PHA) (11249738001, Sigma), QUANTI-Blue solution (rep-qbs, InvivoGen), tofacitinib (FT32555, Biosynth), WST-1 reagent (11644807001, Merck), mIL-6 (Quantikine ELISA, M6000B, R&D Systems), MCP-1 (Quantikine ELISA, JE00B, R&D Systems), and CXCL1 (DuoSet ELISA, DY453, R&D Systems).

Neutralization of TNF-α-Mediated Cytotoxicity in Mouse Fibrosarcoma L929 Cells

Mouse fibrosarcoma L929 cells were cultured in DMEM supplemented with 10% FBS and 1% Penicillin−Streptomycin at 37 °C, 5% CO_2. Cells were gently rinsed with prewarmed PBS, detached with 0.05% Trypsin for 2−3 min at 37 °C, briefly centrifuged to pellet, resuspended in complete DMEM media, and counted. L929 cells were seeded in 96-well plates (5000 cells per well) in complete media and incubated for 48 h at 37 °C, 5% CO_2. Then, cells were treated with dilution series of SDCs or controls, followed by actinomycin D (1 μg/mL) and human TNF-α (0.3 ng/mL), and incubated at 37 °C for 24 h. Cell viability was measured using the WST-1 reagent as per manufacturer's instructions and incubated for 24 h. Absorbance was measured at 450 nM and percentage of cell viability was calculated compared to untreated cells (n = 4). IC_{50} was calculated using four-parameter nonlinear regression in GraphPad Prism.

HEK-Blue IL-23 Reporter Assay

Cells were cultured in DMEM supplemented with 10% FBS, 1% Normocin and 1% Penicillin−Streptomycin at 37 °C, 5% CO_2. Assays were carried out in 96-well plates, seeding 50,000 cells per well in DMEM supplemented with 10% FBS and 1% Penicillin−Streptomycin. Dilution series of SDC covering from 5 μM to 85 pM were preincubated with or without 50 nM of HNE for 24 h at 37 °C. Then, cells were incubated with 1 ng/mL of human IL23 and test articles for 24 h at 37 °C. STAT3 activation was measured via SEAP reporter gene activity using the QUANTI-Blue solution colorimetric reagent as per manufacturer's instructions. Percentage of neutralization was calculated considering an OD_{595} of 5 μM of tofacitinib and human IL23-stimulated cells as maximum and minimum inhibition, respectively. IC_{50} was calculated using four-parameter nonlinear regression in GraphPad Prism.

HEK-Blue IL-12 Reporter Assay

Cells were cultured in DMEM supplemented with 10% FBS, 1% Normocin and 1% Penicillin−Streptomycin at 37 °C, 5% CO_2. Assays were carried out in 96-well plates, seeding 50,000 cells per well in DMEM supplemented with 10% FBS and 1% Penicillin−Streptomycin. Dilution series of SDC covering from 2 μM to 113 pM were preincubated with HNE at 50 nM for 24 h at 37 °C. Then, cells were incubated with 30 ng/mL of cynomolgus IL-12 and test articles for 24 h at 37 °C. STAT4 activation was measured via SEAP reporter gene activity using the QUANTI-Blue solution colorimetric reagent as per manufacturer's instructions. Percentage of neutralization was calculated considering an OD_{595} of 2 μM of tofacitinib and cynomolgus IL-12-stimulated cells as maximum and minimum inhibition, respectively. IC_{50} was calculated using four-parameter nonlinear regression in GraphPad Prism.

Inhibition of PHA-Mediated Proliferation of Human PBMCs

Healthy human PBMCs were cultured in RPMI supplemented with 10% FBS and 1% Penicillin−Streptomycin at 37 °C, 5% CO_2. Assays were carried out in 96-well plates, seeding 100,000 cells per well. PBMCs were stimulated with 2 μg/mL of PHA and incubated with tofacitinib, SDC, or control in the presence or absence of 50 nM of HNE for 72 h at 37 °C, 5% CO_2. First PBMC sample was incubated with 4 μM of tofacitinib, 1 μM of SDC, or 1 μM of control, whereas additional four PBMC samples were incubated with 40 μM of tofacitinib or 10 μM of SDC. Cellular proliferation was measured by incubation with the WST-1 colorimetric reagent as per manufacturer's instructions for 5 h. Absorbance was measured at 450 nM and percentage of neutralization was calculated considering an OD_{450} of 100 μM and 564 pM of tofacitinib as maximum and minimum inhibition, respectively.

LPS-Induced Acute Inflammation Study in Tg1278TNFKOhTNFR1KI Mice

The study was carried out by Biomedcode Hellas SA, Greece. The test facility is accredited by the Hellenic republic directorate of Agricultural and Veterinary Policy of the Attica Region to conduct research in laboratory animals. All the conditions of testing conformed to the Presidential Decree No 56/2013 Governmental Gazette No A′ 106 applicable in Greece, which is the implementation of the EEC Directive 2010/63/EEC, and were approved by the Directorate of Agricultural and Veterinary Policy (DAVP) of the Attica Region (Approval license Protocol No. 466360/25-05-22). Test articles were diluted in PBS to 0.1 mg/mL so that a dose volume of 10 mL/kg would give dosing at 1 mg/kg based on body weight of each individual mouse. Each group consisted of 8 mice. Test articles were administered intraperitoneally as a single dose 2 h before LPS administration. After 2 h, 10 μg of LPS was administered intraperitoneally to each mouse. After a further 5 h, animals were euthanized and terminal blood was collected by cardiac puncture. Blood was allowed to clot and then a serum-containing supernatant was collected after centrifugation. Levels of pro-inflammatory cytokines mIL6, mMCP-1, and mCXCL1 were measured by ELISA, following manufacturer's instructions. Standards curves were prepared for each cytokine and serum was diluted 1:400 for mIL6 and mMCP-1 and 1:200 for mCXCL1.

Tg197 Transgenic Mouse Model of Polyarthritis

The study was carried out by Biomedcode Hellas SA, Greece (Directorate of Agricultural and Veterinary Policy (DAVP) of the Attica Region Approval license Protocol No. 1139048/09-11-2022). At 3 weeks of age, prior to the establishment of arthritis pathology, mice were treated with test articles subcutaneously at 10 μL/g of body weight. Experimental groups containing 10 sex- and age-matched mice were treated with vehicle (PBS), ELN22-108, ELN28-135-01, or ELN0-2V-135-01 (isotype control). For administration, test articles were diluted in PBS to 0.3 mg/mL concentrations to allow dosing at 3 mg/kg. Animals were weighed using an electronic scale on the day of dosing to determine necessary volume to achieve correct dose. Animals were dosed twice a week for 7 weeks to give a total duration of the study of 10 weeks. Arthritic score was recorded once a week for each ankle joint using a set of characteristics and a scale of 0−3 (0 = no disease, 0.5 = mild disease, 1 = mild to moderate disease, 1.5 = moderate disease, 2 = moderate to severe disease, 2.5 severe disease, 3 = very severe disease). An additional group of 4 mice was left untreated and sacrificed at 3 weeks of age to serve as a control group. At the end of the study, mice were sacrificed, and hind ankle joints were collected. The right ankle joints were processed for histopathological evaluation and the left ankle joints were snap-frozen in liquid nitrogen for RNaseq analysis. In addition, blood was collected via cardiac puncture, allowed to clot for 20 min at RT, and the supernatant was harvested after centrifugation. The concentration of mCXCL1 and mMCP-1 was assessed in all serum samples by using DuoSet ELISA kits from R&D Systems (DY453 and DY479), following manufacturer's indications. In both cases, serum samples were diluted 1:25 in reagent buffer and concentrations were calculated based on a standard curve.

Histopathological Evaluation of Ankle Joints from a Tg197 Transgenic Mouse Model

Hind ankle joints from the Tg197 transgenic mouse model of polyarthritis study were collected when mice were sacrificed at week 10. The right ankle joints were processed for histopathological evaluation as follows: the skin was removed, and the sample was fixed in 4% aqueous formaldehyde solution at RT overnight. Demineralization was then performed by incubating samples with 13% EDTA in 0.1 M sodium phosphate at RT for 30 days. Samples were embedded in paraffin in the sagittal plane, sectioned using a microtome, and

https://doi.org/10.1021/acs.jmedchem.6c00532
J. Med. Chem. 2026, 69, 9664−9679

slides were generated. Slides were stained with H&E (hematoxylin and eosin stain), TRAP, or safranin O to evaluate inflammation, bone erosion, and cartilage destruction, respectively. In each case, histopathology severity for each individual ankle joint was scored blindly using a scale of 0−3. Total histopathology score was calculated by adding all individual scores.

Bulk RNA Sequencing (RNA-Seq)

The left ankle joint of four mice per group and four 10 week-old wild type littermate mice were used for differential gene expression analysis. Total RNA was extracted from each sample using the Trizol reagent, and RNA-Seq was carried out. Raw FASTQ files were generated using standard pipelines and subjected to quality controls. These controls included using FastQC, followed by subsequent trimming of poor-quality bases with TrimGalore and removing polyA tails using the respective functionality of TrimGalore. Reads were aligned on the UCSC mm10 reference genome using Hisat2 and Bowtie2. The resulting BAM files from each mapping round were merged using samtools and gene counts were quantified with FeatureCounts on a primary annotation (GRCm38.p6, gencode release M23, ensembl release 98). Differential gene expression for 14432 genes was analyzed with DESeq2. DEGs were defined based on the following standard thresholds: absolute logFC against control ≥ 1 and an adjusted p-value (corrected for multiple comparisons at FDR of 5%) ≤ 0.05. By comparing the 10 week vehicle-treated mice (referred as disease) to the 10 week wild-type control mice (referred as Wt), 2736 disease-associated DEGs were identified. The differential gene expression of these 2736 genes was compared for ELN22-108, ELN28-135-01, and ELN0-2V-135-01 and represented in two-dimensional scatterplots. Log fold change of disease vs control (Wt) (x-axis) was plotted against the log2 fold change of treatment group vs Wt (y-axis).

Affinity Measurements of SDCs and Precursors to TNF-α by Bio-Layer Interferometry

BLI was carried on a Sartorius Octet R8 Protein Analysis System. SA streptavidin biosensors (Satorius, 18-5020) were hydrated for 10 min with 0.1% BSA in PBST (PBS with 0.1% Tween 20) buffer and loaded with 10 nM of biotinylated TNF-α for 300 s. Then, biosensors were dipped for 2700 s (association) into 2-fold dilution series of ELN22-108, ELN22-135, and ELN28-135-01 covering from 2 nM to 0.03 nM, followed by 2700 s into 0.1 BSA in PBST (dissociation). Kinetic analysis was performed with Octet BLI Analysis software using a global, 1:1 fit model, considering ka (1/Ms) and kdis (1/s).

■ ASSOCIATED CONTENT

Supporting Information

The Supporting Information is available free of charge at https://pubs.acs.org/doi/10.1021/acs.jmedchem.6c00532.

Molecular formula strings and SMILES for all compounds (CSV)

Additional experimental results (PDF)

■ AUTHOR INFORMATION

Corresponding Author

Obinna C. Ubah − *Elasmogen Ltd., Aberdeen AB25 2ZP, U.K.;* orcid.org/0000-0001-9011-8405; Email: obinna.ubah@elasmogen.com

Authors

Euan Murray − *Elasmogen Ltd., Aberdeen AB25 2ZP, U.K.*

Stella Priyanka − *Elasmogen Ltd., Aberdeen AB25 2ZP, U.K.*

Julia Martinez-Fraile − *Elasmogen Ltd., Aberdeen AB25 2ZP, U.K.*

Ruslan Grygorash − *Abzena Ltd., Babraham Research Campus, Cambridge CB22 3AT, U.K.*

Mohannad Idress − *Abzena Ltd., Babraham Research Campus, Cambridge CB22 3AT, U.K.;* orcid.org/0000-0002-3928-3365

Luke C. Brownbridge − *Abzena Ltd., Babraham Research Campus, Cambridge CB22 3AT, U.K.*

Stella Glavina − *Abzena Ltd., Babraham Research Campus, Cambridge CB22 3AT, U.K.*

Nicolas Camper − *Abzena Ltd., Babraham Research Campus, Cambridge CB22 3AT, U.K.*

Robert Boyd − *Elasmogen Ltd., Aberdeen AB25 2ZP, U.K.*

Andrew J. Porter − *Elasmogen Ltd., Aberdeen AB25 2ZP, U.K.; School of Medical Sciences, Scottish Biologics Facility, University of Aberdeen, Aberdeen AB25 2ZP, U.K.*

Caroline J. Barelle − *Elasmogen Ltd., Aberdeen AB25 2ZP, U.K.*

Complete contact information is available at: https://pubs.acs.org/10.1021/acs.jmedchem.6c00532

Author Contributions

‖E.M., S.P., and J.M.F. contributed equally to this work. E.M., S.P., and J.M.F. performed the in vitro functional assays. E.M., S.P., J.M.F., and O.C.U. analyzed, interpreted, and presented the in vivo efficacy studies, including serum cytokine analyses. R.G. synthesized the linker payload. M.I. prepared the bioconjugates. L.C.B. and S.G. performed neutrophil elastase payload release assays and plasma stability studies. O.C.U., C.J.B., A.J.P, and R.B. contributed to the conceptualization and design of the study, with O.C.U. leading key aspects of idea generation, study conception, and shaping the overall scientific direction. O.C.U., E.M., J.M.F., and N.C. wrote the manuscript, with all authors contributing to the final version.

Notes

The authors declare the following competing financial interest(s): O.C.U., E.M., S.P., J.M.F., R.B., A.J.P. and C.J.B. are employees of Elasmogen Limited. Elasmogen Ltd paid Abzena Ltd for its synthetic chemistry, bioconjugation and analytical services. R.G., M.I., L.C.B., S.G. and N.C. are employees of Abzena Ltd.

■ ACKNOWLEDGMENTS

This work was supported by the UKRI FLF/MRC Award MR/V026283/1 (O.C.U.) and UKRI2085 (O.C.U.).

■ ABBREVIATIONS USED

α1-AT, alpha-1-antitrypsin; ADA, antidrug antibody; ADC, antibody drug conjugate; BLI, biolayer interferometry; CCL2, chemokine (C−C motif) ligand 2; CHO, Chinese hamster ovary; CXCL1, C-X-C motif chemokine ligand 1; CXCL5, C-X-C motif chemokine ligand 5; CXCL13, C-X-C motif chemokine ligand 13; DAR, drug-to-antibody ratio; DEGs, differentially expressed genes; DHAA, dehydroascorbic acid; DMEDA, *N*,*N*′-dimethylethylenediamine; DMEM, Dulbecco's Modified Eagle's Medium; EU/mg, endotoxin units per milligram; FBS, fetal bovine serum; FcRn, neonatal Fc receptor; GRM, glucocorticoid receptor modulator; HATU, hexafluorophosphate azabenzotriazole tetramethyl uronium; H&E, hematoxylin and eosin stain; HIC, hydrophobic interaction chromatography; HMW, high molecular weight; HNE, human neutrophil elastase; HS, hidradenitis suppurativa; IBD, inflammatory bowel disease; IL-6, interleukin-6; IL-12, interleukin-12; IL-23, interleukin-23; IL12Rβ1, interleukin-12

https://doi.org/10.1021/acs.jmedchem.6c00532
J. Med. Chem. 2026, 69, 9664−9679

receptor β1; IL23R, interleukin-23 receptor; IMIDs, immune-mediated inflammatory diseases; JAK, Janus kinase; JAK2, Janus kinase 2; JAKi, Janus kinase inhibitor; LAL, Limulus amebocyte lysate; Mal, maleimide; MCP-1, monocyte chemoattractant protein 1; MMP3, matrix metalloproteinase-3; MMP13, matrix metalloproteinase-13; MNE, mouse neutrophil elastase; ND50, 50% neutralization dose; NE, neutrophil elastase; PAB, *p*-aminobenzyl alcohol; PBMCs, peripheral blood mononuclear cells; PHA, phytohemagglutinin-L; PNP, *p*-nitrophenyl; PsA, psoriatic arthritis; PsO, psoriasis; RA, rheumatoid arthritis; RNA-Seq, RNA sequencing; RP, reversed phase; sTNF-α, soluble TNF-α; SDC, soloMER drug conjugate; SEAP, secreted embryonic alkaline phosphatase; SEM, standard error of the mean; SOCS1, suppressor of cytokine signaling 1; STAT, signal transducer and activator of transcription; STAT3, signal transducer and activator of transcription 3; STAT4, signal transducer and activator of transcription 4; tmTNF-α, transmembrane TNF-α; TRAP, tartrate-resistant acid phosphatase; Tyk2, tyrosine kinase 2; VIST, V-domain Ig suppressor of T-cell activation

REFERENCES

(1) Conrad, N.; Misra, S.; Verbakel, J. Y.; et al. Incidence, prevalence, and co-occurrence of autoimmune disorders over time and by age, sex, and socioeconomic status: A population-based cohort study of 22 million individuals in the UK. *Lancet* **2023**, *401* (10391), 1878−1890.

(2) Blandizzi, C.; Gionchetti, P.; Armuzzi, A.; Caporali, R.; Chimenti, S.; Cimaz, R.; Cimino, L.; Lapadula, G.; Lionetti, P.; Marchesoni, A.; et al. The role of tumour necrosis factor in the pathogenesis of immune-mediated diseases. *Int. J. Immunopathol. Pharmacol.* **2014**, *27* (1_suppl), 1−10.

(3) Jang, D.; Lee, A.; Shin, H.; et al. The role of tumor necrosis factor alpha (TNF-alpha) in autoimmune disease and current TNF-alpha inhibitors in therapeutics. *Int. J. Mol. Sci.* **2021**, *22* (5), 2719.

(4) Roda, G.; Jharap, B.; Neeraj, N.; Colombel, J. Loss of response to anti-TNFs: Definition, epidemiology, and management. *Clin. Transl. Gastroenterol.* **2016**, *7* (1), No. e135.

(5) McPherson, M. J.; Hobson, A. D.; Hernandez, A., Jr; Marvin, C. C.; Waegell, W.; Goess, C.; Oh, J. Z.; Shi, D.; Hayes, M. E.; Wang, L.; et al. An anti−TNF−glucocorticoid receptor modulator antibody-drug conjugate is efficacious against immune-mediated inflammatory diseases. *Sci. Transl. Med.* **2024**, *16* (739), No. eadd8936.

(6) Zhao, Q. Bispecific antibodies for autoimmune and inflammatory diseases: Clinical progress to date. *BioDrugs* **2020**, *34* (2), 111−119.

(7) Ntari, L.; Nikolaou, C.; Kranidioti, K.; et al. Combination of subtherapeutic anti-TNF dose with dasatinib restores clinical and molecular arthritogenic profiles better than standard anti-TNF treatment. *J. Transl. Med.* **2021**, *19* (1), 165−y.

(8) Hu, X.; Li, J.; Fu, M.; Zhao, X.; Wang, W. The JAK/STAT signaling pathway: From bench to clinic. *Signal Transduct Target Ther* **2021**, *6* (1), 402.

(9) Bonelli, M.; Kerschbaumer, A.; Kastrati, K.; et al. Selectivity, efficacy and safety of JAKinibs: New evidence for a still evolving story. *Ann. Rheum. Dis.* **2024**, *83* (2), 139−160.

(10) Boyle, D. L.; Soma, K.; Hodge, J.; et al. The JAK inhibitor tofacitinib suppresses synovial JAK1-STAT signalling in rheumatoid arthritis. *Ann. Rheum. Dis.* **2015**, *74* (6), 1311−1316.

(11) Boyadzhieva, Z.; Ruffer, N.; Burmester, G.; Pankow, A.; Krusche, M. Effectiveness and safety of JAK inhibitors in autoinflammatory diseases: A systematic review. *Frontiers in Medicine* **2022**, *9*, 930071.

(12) Spinelli, F. R.; Meylan, F.; O'Shea, J. J.; Gadina, M. JAK inhibitors: Ten years after. *Eur. J. Immunol.* **2021**, *51* (7), 1615−1627.

(13) Tokareva, K.; Reid, P.; Yang, V.; et al. JAK inhibitors and black box warnings: What is the future for JAK inhibitors? *Expert Rev. Clin. Immunol.* **2023**, *19* (11), 1385−1397.

(14) Buttgereit, F.; Aelion, J.; Rojkovich, B.; et al. Efficacy and safety of ABBV-3373, a novel anti−tumor necrosis factor glucocorticoid receptor modulator antibody−drug conjugate, in adults with moderate-to-severe rheumatoid arthritis despite methotrexate therapy: A randomized, Double-Blind, active-controlled Proof-of-Concept phase IIa trial. *Arthritis Rheumatol.* **2023**, *75* (6), 879−889.

(15) Riaz, B.; Sohn, S. Neutrophils in inflammatory diseases: Unraveling the impact of their derived molecules and heterogeneity. *Cells* **2023**, *12* (22), 2621.

(16) Brostjan, C.; Oehler, R. The role of neutrophil death in chronic inflammation and cancer. *Cell Death Discovery* **2020**, *6* (1), 26.

(17) Doring, G. The role of neutrophil elastase in chronic inflammation. *Am. J. Respir. Crit. Care Med.* **1994**, *150* (6_pt_2), 114−S117.

(18) Mohamed Amar, I. A.; Huvelle, S.; Douez, E.; et al. Dual intra- and extracellular release of monomethyl auristatin E from a neutrophil elastase-sensitive antibody-drug conjugate. *Eur. J. Med. Chem.* **2022**, *229*, 114063.

(19) Raposo Moreira Dias, A.; Pina, A.; Dean, A.; et al. Neutrophil elastase promotes linker cleavage and paclitaxel release from an integrin-targeted conjugate. *Chemistry* **2019**, *25* (7), 1696−1700.

(20) Ubah, O. C.; Lake, E. W.; Ott, K. L.; et al. The structural basis for the selective antagonism of soluble TNF-alpha by shark variable new antigen receptors. *Nat. Commun.* **2025**, *17*, .

(21) Nuttall, S. D. Overview and discovery of IgNARs and generation of VNARs. *Single Domain Antibodies: Methods and Protocols* **2012**, *911*, 27−36.

(22) Zielonka, S.; Empting, M.; Grzeschik, J.; Könning, D.; Barelle, C. J.; Kolmar, H. Structural insights and biomedical potential of IgNAR scaffolds from sharks. *mAbs* **2015**, *7* (1), 15−25.

(23) Liu, C.; Lin, H.; Cao, L.; Wang, K.; Sui, J. Research progress on unique paratope structure, antigen binding modes, and systematic mutagenesis strategies of single-domain antibodies. *Front. Immunol.* **2022**, *13*, 1059771.

(24) Kovalenko, O. V.; Olland, A.; Piché-Nicholas, N.; et al. Atypical antigen recognition mode of a shark immunoglobulin new antigen receptor (IgNAR) variable domain characterized by humanization and structural analysis. *J. Biol. Chem.* **2013**, *288* (24), 17408−17419.

(25) Ubah, O. C.; Lake, E. W.; Gunaratne, G. S.; Gallant, J. P.; Fernie, M.; Robertson, A. J.; Marchant, J. S.; Bold, T. D.; Langlois, R. A.; Matchett, W. E.; et al. Mechanisms of SARS-CoV-2 neutralization by shark variable new antigen receptors elucidated through X-ray crystallography. *Nat. Commun.* **2021**, *12* (1), 7325.

(26) Ubah, O. C.; Steven, J.; Kovaleva, M.; et al. Novel, anti-hTNF-alpha variable new antigen receptor formats with enhanced neutralizing potency and multifunctionality, generated for therapeutic development. *Front. Immunol.* **2017**, *8*, 1780.

(27) Ubah, O. C.; Steven, J.; Porter, A. J.; Barelle, C. J. An anti-hTNF-alpha variable new antigen receptor format demonstrates superior in vivo preclinical efficacy to humira(R) in a transgenic mouse autoimmune polyarthritis disease model. *Front. Immunol.* **2019**, *10*, 526.

(28) Ubah, O. C.; Porter, A. J.; Barelle, C. J. In vitro ELISA and cell-based assays confirm the low immunogenicity of VNAR therapeutic constructs in a mouse model of human RA: An encouraging milestone to further clinical drug development. *J. Immunol. Res.* **2020**, *2020*, 7283239.

(29) Kaempffe, A.; Dickgiesser, S.; Rasche, N.; et al. Effect of conjugation site and technique on the stability and pharmacokinetics of antibody-drug conjugates. *J. Pharm. Sci.* **2021**, *110* (12), 3776−3785.

(30) Li, J. Y.; Perry, S. R.; Muniz-Medina, V.; et al. A biparatopic HER2-targeting antibody-drug conjugate induces tumor regression in primary models refractory to or ineligible for HER2-targeted therapy. *Cancer Cell* **2016**, *29* (1), 117−129.

https://doi.org/10.1021/acs.jmedchem.6c00532
J. Med. Chem. 2026, 69, 9664−9679

(31) Sussman, D.; Westendorf, L.; Meyer, D. W.; et al. Engineered cysteine antibodies: An improved antibody-drug conjugate platform with a novel mechanism of drug-linker stability. *Protein Eng. Des Sel* **2018**, *31* (2), 47−54.
(32) Steven, J.; Müller, M. R.; Carvalho, M. F.; Ubah, O. C.; Kovaleva, M.; Donohoe, G.; Baddeley, T.; Cornock, D.; Saunders, K.; Porter, A. J.; et al. In vitro maturation of a humanized shark VNAR domain to improve its biophysical properties to facilitate clinical development. *Front. Immunol.* **2017**, *8*, 1361.
(33) Steven, J.; Ubah, O. C.; Buschhaus, M.; et al. In vitro maturation of a humanized shark VNAR domain to improve its biophysical properties. In *Genotype Phenotype Coupling: Methods and Protocols*; Springer, 2019; pp 115−142.
(34) Curciarello, R.; Sobande, T.; Jones, S.; Giuffrida, P.; Di Sabatino, A.; Docena, G. H.; MacDonald, T. T.; Kok, K. Human neutrophil elastase proteolytic activity in ulcerative colitis favors the loss of function of therapeutic monoclonal antibodies. *J. Inflammation Res.* **2020**, *13*, 233−243.
(35) Moore, A. R.; Appelboam, A.; Kawabata, K.; et al. Destruction of articular cartilage by alpha2macroglobulin elastase complexes: Role in rheumatoid arthritis. *Ann. Rheum. Dis.* **1999**, *58* (2), 109−113.
(36) Navrazhina, K.; Garcet, S.; Zheng, X.; Hur, H. B.; Frew, J. W.; Krueger, J. G. High inflammation in hidradenitis suppurativa extends to perilesional skin and can be subdivided by lipocalin-2 expression. *J. Allergy Clin. Immunol.* **2022**, *149* (1), 135−144e12.
(37) Ghosh, A. K.; Brindisi, M. Organic carbamates in drug design and medicinal chemistry. *J. Med. Chem.* **2015**, *58* (7), 2895−2940.
(38) Keffer, J.; Probert, L.; Cazlaris, H.; et al. Transgenic mice expressing human tumour necrosis factor: A predictive genetic model of arthritis. *EMBO J.* **1991**, *10* (13), 4025−4031.
(39) Hobson, A. D.; McPherson, M. J.; Hayes, M. E.; et al. Discovery of ABBV-3373, an anti-TNF glucocorticoid receptor modulator immunology antibody drug conjugate. *J. Med. Chem.* **2022**, *65* (23), 15893−15934.
(40) Rothstein, J.; Carriere, C.; Bell, K.; et al. Pos0666 immune-targeted glucocorticoid adc for the treatment of autoimmune and inflammatory diseases. *Ann. Rheum. Dis.* **2025**, *84*, 850−851.
(41) Dittrich, A. S.; Kühbandner, I.; Gehrig, S.; Rickert-Zacharias, V.; Twigg, M.; Wege, S.; Taggart, C.; Herth, F.; Schultz, C.; Mall, M. A. Elastase activity on sputum neutrophils correlates with severity of lung disease in cystic fibrosis. *Eur. Respir. J.* **2018**, *51* (3), 1701910.
(42) El-Eshmawy, M. M.; El-Adawy, E. H.; Mousa, A. A.; Zeidan, A. E.; El-Baiomy, A. A.; Abdel-Samie, E. R.; Saleh, O. M. Elevated serum neutrophil elastase is related to prehypertension and airflow limitation in obese women. *BMC Women's Health* **2011**, *11* (1), 1.
(43) Thulborn, S. J.; Mistry, V.; Brightling, C. E.; Moffitt, K. L.; Ribeiro, D.; Bafadhel, M. Neutrophil elastase as a biomarker for bacterial infection in COPD. *Respir. Res.* **2019**, *20* (1), 170.
(44) Schaaf, B.; Wieghorst, A.; Aries, S.; Dalhoff, K.; Braun, J. Neutrophil inflammation and activation in bronchiectasis: Comparison with pneumonia and idiopathic pulmonary fibrosis. *Respiration* **2000**, *67* (1), 52−59.
(45) Zeng, W.; Song, Y.; Wang, R.; He, R.; Wang, T. Neutrophil elastase: From mechanisms to therapeutic potential. *J. Pharm. Anal.* **2023**, *13* (4), 355−366.
(46) Lee, W. L.; Downey, G. P. Leukocyte elastase: Physiological functions and role in acute lung injury. *Am. J. Respir. Crit. Care Med.* **2001**, *164* (5), 896−904.
(47) Ahmed, N. T.; Kummarapurugu, A. B.; Zheng, S.; et al. Neutrophil elastase targets select proteins on human blood-monocyte-derived macrophage cell surfaces. *Int. J. Mol. Sci.* **2024**, *25* (23), 13038.
(48) Alley, S. C.; Benjamin, D. R.; Jeffrey, S. C.; et al. Contribution of linker stability to the activities of anticancer immunoconjugates. *Bioconjug Chem.* **2008**, *19* (3), 759−765.
(49) Szijj, P. A.; Bahou, C.; Chudasama, V. Minireview: Addressing the retro-michael instability of maleimide bioconjugates. *Drug Discov Today Technol.* **2018**, *30*, 27−34.
(50) Fontaine, S. D.; Reid, R.; Robinson, L.; Ashley, G. W.; Santi, D. V. Long-term stabilization of maleimide-thiol conjugates. *Bioconjug Chem.* **2015**, *26* (1), 145−152.
(51) Valli, A.; Kuuliala, K.; Virtanen, A.; et al. Tofacitinib treatment modulates the levels of several inflammation-related plasma proteins in rheumatoid arthritis and baseline levels of soluble biomarkers associate with the treatment response. *Clin. Exp. Immunol.* **2022**, *210* (2), 141−150.
(52) Zhao, J.; Zhang, B.; Mao, Q.; et al. Discovery of a colon-targeted azo prodrug of tofacitinib through the establishment of colon-specific delivery systems constructed by 5-ASA-PABA-MAC and 5-ASA-PABA-diamine for the treatment of ulcerative colitis. *J. Med. Chem.* **2022**, *65* (6), 4926−4948.

https://doi.org/10.1021/acs.jmedchem.6c00532
J. Med. Chem. 2026, 69, 9664−9679